UNIVERSIDAD DE CONCEPCIÓN
FACULTAD DE CIENCIAS FÍSICAS Y MATEMÁTICAS

A SYSTEMATIC METHOD TO IDENTIFY RUNAWAYS FROM STAR CLUSTERS PRODUCED FROM SINGLE-BINARY INTERACTIONS:

A CASE STUDY OF M67

Por: Alonso Eduardo Herrera Urquieta

Thesis presented to the Faculty of Physical and Mathematical Sciences of the Universidad de Concepción for the academic degree of Magíster in Astronomy.

Enero 2024
Concepción, Chile

Profesor Guía: Nathan William Cecil Leigh

Dedicada a mi familia que me apoya cada día, y a las maravillosas personas que he tenido la fortuna de encontrar en el camino.

AGRADECIMIENTOS

Quiero expresar mi más sincera gratitud a quienes me han acompañado a lo largo del vertiginoso camino universitario.

A mis padres, por su amor, su apoyo y su confianza. Gracias por creer en mí y por ayudarme a crear y alcanzar mis metas. Sin ustedes no habría podido estudiar con la total libertad que me permitió terminar mi carrera como también potenciar mis habilidades más allá de lo meramente académico.

A mis fieles amigos, Patricio, Gonzalo y Lukas, por su inquebrantable amistad y con quienes he crecido. Siempre celebrando nuestros logros y apoyándonos en los retos que nos ha dado la adultez. Su compañia, lealtad, cariño y humor son invaluables para mí.

No olvido también a quienes tomamos la decisión de dedicarnos a la astronomía durante el año 2017 y nos apoyamos hasta el final del arduo trayecto. Sin ustedes todo habría sido mucho más difícil. Además doy gracias a quienes me acompañaron en la labor de ser parte del centro de estudiantes de la carrera durante 4 años.

Agradezco a mi tuna, la Tuna de la Universidad de Concepción, por brindarme el espacio que necesitaba en mi vida. La cual en estos dos años me enseño mi verdadero potencial, donde puedo ser yo mismo, disfrutando de la bohemia universitaria. Conocí personas únicas con las cuales he vivido experiencias inolvidables.

A mi profesor guía, Nathan Leigh, por su orientación, su paciencia y su sabiduría. Gracias por ayudarme a crecer como científico y como persona, y por sobre todo alentarme a terminar mi magíster.

Y finalmente, y no menos importante a Nayadette, mi novia, con quien a la publicación de esta tesis ya tendremos un año de estar juntos. Me cuesta poner en palabras lo mucho que me ayudó encontrarte en mi vida. Me diste un amor incondicional, celebraste mis logros con alegría y me diste cobijo en los momentos difíciles. Te agradezco con todo mi ser y estoy ansioso de seguir avanzando en nuestras vidas juntos.

Acknowledgments

I want to express my sincere thanks to all the collaborators for their guidance in this investigation. Special thanks to Aaron M. Geller, Taeho Ryu, Silvia Toonen, Robert D. Mathieu, Marina Kounkel, Steffani M. Grondin and Jeremy J. Webb. AEHR acknowledges financial support from Millenium Nucleus NCN19_058 (TITANs). Gratefully acknowledges the generous support of a Fondecyt General grant 1230082, as well as support from Millenium Nucleus NCN19_058 (TITANs) and funding via the BASAL Centro de Excelencia en Astrofisica y Tecnologias Afines (CATA) grant PFB-06/2007. I also thanks support from ANID BASAL project ACE210002 and ANID BASAL projects ACE210002 and FB210003.

Resumen

Las estrellas fugitivas o "Runaway Stars" son estrellas que se cree, han sido expulsadas de sus respectivos cúmulos estelares con altas velocidades relativas al movimiento del centro de masa del cúmulo. Existen dos mecanismos para su producción: expulsiones basadas en supernovas en sistemas binarios, donde la estrella compañera explota sin dejar un remanente y lanza a la otra a una velocidad orbital instantánea, y la desintegración de sistemas triples (o sistemas múltiples de orden superior) que produce una estrella binaria fugitiva, Runaway Binary (RB) y una estrella fugitiva solitaria, Runaway Star (RS).

Después de discutir las expectativas teóricas para ambos mecanismos, buscamos candidatos a estrellas fugitivas utilizando datos del telescopio espacial Gaia DR3, con enfoque en la desintegración triple en el antiguo cúmulo abierto M67. **Creamos una metodología sistemática para buscar pares candidatos de RS/RB producidos por la desintegración de sistemas de tres cuerpos ligados**, formados a partir de interacciones entre sistema binario y una estrella solitaria, basada en la conservación del momentum y la causalidad. El método es generalizado y puede ser aplicado a cualquier cúmulo que tenga un conjunto de datos cinemáticos 5D. Utilizamos diversos criterios para buscar estos pares en un campo de visión circular de 150 pc alrededor del cúmulo abierto M67, el cual es utilizado como cúmulo de referencia para probar la robustez de nuestro método. **Nuestros resultados revelan solo un par de RS/RB que es consistente con todos nuestros criterios de selección**, de un tamaño de muestra inicial de 10^8 pares (es decir, 10^4 objetos).

Keywords – estrellas: cinemática – mecánica celeste, Dinámica estellar – Medio interestelar: cinemática y dinámica

Abstract

Runaway stars are thought to have been ejected from star clusters with high velocities relative to the cluster centre-of-mass motion. There are two competing mechanisms for their production: supernova-based ejections in binaries, where one companion explodes leaving no remnant and launching the other companion at the instantaneous orbital velocity, and the disintegration of triples (or higher-order multiples) producing a recoiled runaway binary (RB) and a runaway star (RS). After discussing the theoretical expectations for both mechanisms, we search for runaway star candidates using data from the Gaia DR3 survey, with a focus on triple disintegration in the old open cluster M67. **We create a systematic methodology to look for candidate RS/RB runaway pairs produced from the disintegration of bound three-body systems formed from single-binary interactions**, based on momentum conservation and causality. The method is general, and can be applied to any cluster having a 5D kinematic data set. We use our criteria to search for these pairs in a 150 pc circular field of view surrounding the open cluster M67, which we use as a benchmark cluster to test the robustness of our method. **Our results reveal only one RS/RB pair that is consistent with all of our selection criteria**, out of an initial sample size of $\sim 10^8$ pairs (i.e., $\sim 10^4$ objects).

Keywords – stars: kinematics – celestial mechanics, stellar dynamics – ISM: kinematics and dynamics

Contents

List of Tables

List of Figures

Chapter 1

Introduction

Star clusters with large stellar densities $\gtrsim 100\ M_{\odot} pc^{-3}$ create very active dynamical environments, where binary and single stars interact on short timescales of order a few Myrs (e.g. Leigh and Sills, 2011; Leigh and Geller, 2012). Such star clusters evolve due to the intracluster dynamics (Reipurth et al., 2010), ejecting stars into the Galactic field via a combination of two-body relaxation and the disintegration of higher-order multiples (usually binaries) interacting (often chaotically) due to single-binary and binary-binary interactions. This binding and then subsequent dissociation of temporary groupings of three or more stars occurs in all types of star clusters, including nuclear star clusters, globular clusters (GCs) and open clusters (OCs). Analogously, it is also possible for stable triple systems to become unstable, ejecting a binary and single star. We expect these events to be relatively rare in dense clusters since here the requirement for dynamical stability favours wide triples which are prone to disruption due to interactions with direct singles and binaries on short timescales.

For especially young clusters, stars can also be ejected from clusters due to supernovae (SN) explosions in binaries, which act to destroy the SN progenitor and launch its binary companion at the instantaneous orbital velocity.

Stars ejected from a cluster due to either of the above mechanisms (i.e., excluding two-body relaxation and other mechanisms that may be operating more rarely) are known as runaway stars (RSs). Observationally, RSs are typically defined as stars with velocities above 30 km s $^{-1}$ (e.g. Blaauw, 1961; Renzo et al., 2019) relative to the host cluster centre-of-mass velocity. But they can have lower velocities as well,

in which case they are typically referred to as walkaway stars (Schoettler et al., 2020). Typical velocities of RSs escaping from young OCs must be sufficiently high to identify them as RSs, but also sufficiently low that they remain sufficiently close to their host cluster to have a non-negligible probability of being observed and associated with a cluster. For the purposes of this investigation, we call *any* object ejected from a cluster due to either the disintegration of triples (formed primarily from single-binary interactions but also including stable multiples that become unstable and disrupt) or the SN-induced ejection scenario as an RS object.

Fast-moving stars have been the subject of extensive studies through both observations and simulations. There have been many studies on dynamically ejected massive stars from young star clusters using numerical integrations (Perets and Šubr, 2012, Fujii and Portegies Zwart, 2014, Oh et al., 2015, Andersson et al. 2020, Dall'Amico et al., 2021). In most cases, the studies were performed using few-body scattering experiments (e.g., Oh et al., 2015, Pflamm-Altenburg and Kroupa, 2006, Gvaramadze and Gualandris, 2010, Gualandris et al., 2004, Ryu et al., 2017d,Ryu et al., 2017a,Ryu et al., 2017c), and focused on young star clusters. Interestingly, however, the contribution of RSs coming from old star clusters relative to the total population of observed fast-moving stars in our Galaxy has been argued to be non-negligible, mostly due to the ejection of singles during three-body interactions (e.g. Weatherford et al., 2023, Grondin et al., 2023a, Grondin et al., 2023b). Observationally, studies of RSs were initially limited to bright massive stars. However, this changed with the launch of the Gaia mission (Gaia Collaboration et al., 2022), which has provided precise measurements of positions and velocities for more than 1.5 billion stars in the Milky Way. As a result, numerous new RSs have been discovered (e.g. Carretero-Castrillo et al., 2023, Liao et al., 2023, Li et al., 2023, Igoshev et al., 2022), including ones at the low-mass end, highlighting the fact that they exist across all stellar masses.

The first scenario for producing RSs involves the explosion of a SN in a binary system (see appendix A2)(Blaauw, 1961). If one binary companion reaches the end of its life first and detonates, leaving behind no remnant, then the secondary will be launched at the instantaneous orbital velocity (e.g. Leigh et al., 2020). The maximum possible velocities of such late-type B-star RSs and G/K dwarfs thought to be produced from binaries disrupted via asymmetric SN explosion are observed to be up to ~ 770 and ~ 1280 km s^{-1} in the galactic rest frame (Tauris, 2014).

Such high velocities are expected to be rare, however. Simulations show that massive RSs resulting from the SN-induced disruption of binaries rarely exceed velocities of 60 km s^{-1}. About 99.8% of the simulated unbound companions are slower than this threshold (Renzo et al., 2019). Most would only barely exceed velocities of 1 km/s (Reipurth et al., 2010). Simulations of low-mass disrupted binaries have shown that, in some rare cases, higher ejection velocities $\lesssim 400$ km s^{-1} can be reached. In old star clusters, we expect the dominant mechanism for producing SN explosions to involve the accretion-induced collapse of white dwarfs (WDs), implying that the progenitor binaries should contain as least one WD companion. The reason for this lack of purely stellar evolution-driven SN is that the cluster turn-off mass tends to be sufficiently low that supernovae are not expected to be occurring anymore. Such compact WD-star binaries should produce high ejection velocities for MS stars, since here the binaries need to be in a near contact state in order to transfer mass to the WD and the WD radius is very small. See the A2 for the maximum ejection velocities possible for the SN-based mechanism for producing RSs when WDs are involved.

The second mechanism for RS production thought to operate in old star clusters is the decay of gravitationally-bound systems of three or four stars. There are two ways to create an RS star via a three-(or four-) body disintegration. In the first scenario, a hierarchical triple (or quadruple) is born stable, but later becomes unstable due to stellar or binary evolution, or even internal secular dynamical processes (e.g., Lidov-Kozai cycles) (e.g. Leigh et al., 2020; Toonen, 2021; Hamers, 2021). In the second scenario, three (or four) bodies meet and become temporarily gravitationally bound via a single-binary (or binary-binary) interaction.

In both scenarios, the triple disintegrates, launching one RS and leaving behind a RB with a recoil velocity decided by linear momentum conservation (Valtonen and Karttunen, 2006; Leigh and Wegsman, 2018). Hence, given an observed RS, using the available observational data, it should be possible to compute exactly where the RB is if it formed from the disintegration of a triple (e.g. Reipurth et al., 2010). It is then possible to search for the RB in large stellar catalogues.

This exercise works well for four-body interactions as well (e.g. Leigh and Geller, 2013; Oh et al., 2015; Leigh et al., 2016a; Ryu et al., 2017b) albeit this requires the identification of *both* ejected singles when the interaction decays into a RB and two RSs. In general, much higher velocities can be produced from triple

disintegrations involving more massive objects, especially if an intermediate-mass black hole is involved (e.g. Colpi et al., 2002, 2003; Leigh et al., 2016b).

We propose a novel methodology for the identification of RS/RB pairs formed from the decay of three-body systems formed from single-binary interactions in a star cluster. As we will show, despite producing similar ejection velocities as the SN-based mechanism, it is these RSs that should be identifiable as being associated with a progenitor cluster with the highest confidence. We leverage the extensive Gaia database to identify the most probable RS/RB pairs. We focus in this investigation on the old open cluster (OC) M67 as a case study, given its close distance to the Sun, moderate age and dynamically active environment. Located at about 860 pc (Cantat-Gaudin et al., 2018) the old OC M67 (NGC 2682) is made up of stars of solar age and composition, with an isochronal age of $\sim$ 4.0 Gyr (VandenBerg and Stetson, 2004; Balaguer-Nunez et al., 2007; Viani and Basu, 2017).

Proper motion and radial velocity surveys of M67 (Yadav et al., 2008; Pasquini et al., 2011; Geller et al., 2015) have confirmed kinematic cluster memberships and estimate a population size of order 1000. Studies have shown that close stellar encounters involving binary stars may be frequent in M67 (Leonard, 1996; Hurley et al., 2005; Leigh and Sills, 2011), and that the formation of these dynamically-sourced populations can also lead to the creation of RSs (e.g. Leigh et al., 2016b).

In Section 2, we present and discuss the relevant physical concepts needed to understand how and why our selectia criteria are constructed. In Section 3, we present our methodology for identifying our most probable RS/RB pairs. In Section 4, we present the results of applying our method to the old OC M67 using the Gaia data, and identify the most probable pairs of RSs/RBs for further study (e.g., radial-velocity observations). Finally, in Section 5 we conclude and discuss improvements on the present analysis that can be implemented when applying our method to other clusters, as well as the significance of our results for confirming the expected dynamical behaviour involving binary stars in clusters by searching for RSs.

Chapter 2

Theoretical Framework

2.1 Theoretical expectations for three-body disintegrations

In this section, we discuss in more detail the observed properties of RSs/RBs ejected from clusters due to single-binary interactions and the underlying physical mechanisms that produce their properties. We show that for the triple disintegration scenario, a larger number of typically robust selection criteria can be applied to the data to constrain the origins of RS/RB pairs, relative to the SN-based mechanism.

In order to quantify what we expect for typical velocities of RSs formed from the triple disintegration scenario, we can compute a theoretically expected distribution of escaper velocities. Let the velocity of the escaper in the centre-of-mass coordinate system be $v_{\rm s}$. Then, a typical escape velocity distribution for the single star in three-body disintegrations can be described by the formula (Valtonen and Karttunen, 2006):

$$f(v_{\rm s})dv_{\rm s} = \frac{(3.5|E_0|^{7/2}m_{\rm s}M/m_{\rm B})v_{\rm s}dv_{\rm s}}{(|E_0| + \frac{1}{2}(m_{\rm s}M/m_{\rm B})v_{\rm s}^2)^{9/2}}, \tag{2.1.1}$$

which is suitable to the isotropic case. Here, the total energy of the three-body system is

$$E_0 = \frac{1}{2} m \dot{r}_{\rm s}^2 + \frac{1}{2} \mathcal{M} \dot{r}^2 - G \frac{m_{\rm a} m_{\rm b}}{r} - G \frac{m_{\rm s} m_{\rm B}}{r_{\rm s}}, \tag{2.1.2}$$

where the separation between the components of the binary system is r and $r_{\rm s}$ is the separation between the escaper and the binary center of mass. For the masses of the bodies we have: $m_{\rm a}$ and $m_{\rm b}$ are the masses of the stars in the binary system, $m_{\rm B}$ is the total binary mass ($m_{\rm a} + m_{\rm b}$), $m_{\rm s}$ is the mass of the escaper and M is the sum of all masses in the three-body system. We also have $\mathcal{M} = \frac{m_{\rm s} m_{\rm b}}{M}$ and $m = \frac{m_{\rm B} m_{\rm s}}{M}$ the reduced masses of the relative motions of the binary and the third body, respectively. The peak of this distribution is obtained by:

$$(v_{\rm s})_{\rm peak} = \sqrt{\frac{2(M - m_{\rm s})}{5 m_{\rm s} M}} \sqrt{|E_0|}. \tag{2.1.3}$$

The most likely escape velocity assuming an initial binary separation of 100 AU, for example, (which is getting close to the expected hard-soft boundary) is of order a few km s^{-1}. Deriving a predicted velocity distribution requires assuming an underlying distribution of binary orbital parameters, both for the triple disintegration scenario as well as for the SN-based mechanism (but see the appendix A2 for more details about the expected ejection velocities for the SN-based mechanism).

Given an assumed ejection velocity for a RS candidate coming from the triple disintegration mechanism, both timescale as well as momentum conservation-based arguments can be used to predict the exact position and velocity of the associated RB candidate. In particular, since momentum conservation should be upheld during the decay of triple systems, the ratio of the RS and RB velocities should be equal to the inverse of the ratio of their masses, or:

$$v_{\rm RB} = \frac{m_{\rm RS}}{m_{\rm RB}} v_{\rm RS}, \tag{2.1.4}$$

where $v_{\rm RS}/v_{\rm RB}$ and $m_{\rm RS}/m_{\rm RB}$ are, respectively, the RS/RB velocities and masses. Given a mass-luminosity ratio, the masses can be converted to observable

luminosities (or magnitudes). Additionally, the candidate RS and its associated candidate RB should have equal travel times from the position where the velocity vectors intersect. We call this position the cross-point, and it should lie within the tidal radius of the host cluster. Finally, using energy conservation, it is in principle possible to also constrain the initial binary orbital separation of the putative single-binary interaction, given observational constraints on the final binary orbital separation as well as all three stellar masses. We emphasize that none of the preceding constraints can be applied to RSs coming from the SN-based mechanism (see the appendix A2 for more details), which should in principle translate into an ability to more confidently associate an identified RS candidate with a host (old) star cluster for the triple disintegration mechanism.

Such dynamical interactions inside clusters can be crucial to deciding the final state of the cluster itself (Andersson et al., 2020). But few constraints on the orbital properties of the underlying binary population are available, particularly in old, massive clusters like GCs with crowded fields of view. We will argue in this investigation that, by looking observationally for the products of single-binary interactions, limits can be placed on the distribution of binary orbital separations. It is possible to obtain these constraints because the mean timescale between single-binary interactions in star cluster cores (where most ejection events are thought to occur) is given by (Leigh and Sills, 2011):

$$\tau_{1+2} = 3.4 \times 10^7 (1 - f_b)^{-1} f_b^{-1} \Big(\frac{1\,\mathrm{pc}}{r_c}\Big)^3 \Big(\frac{10^3\, pc^{-3}}{n_0}\Big)^2 \Big(\frac{v_{rms}}{5\, km\, s^{-1}}\Big) \Big(\frac{m}{1 M_\odot}\Big) \Big(\frac{1 AU}{a}\Big) \mathrm{yr}, \tag{2.1.5}$$

where f_b is the binary fraction, r_c is the core radius in parsecs, n_0 is the number density in the core in pc^{-3}, v_{rms} is the root-mean-square velocity in km/s, m is the average mass (in $\mathrm{M}_\odot$) and a is the mean binary semi-major axis (in AU). Note that Equation 2.1.5 suggests that the rate of single-binary interactions scales linearly with binary semi-major axis, which is the most difficult quantity in this equation to measure observationally. It follows that, by constraining the frequency of RSs formed from single-binary interactions, limits can be placed on the underlying binary orbital separation distribution. Based purely on Equation 2.1.5, it is specifically the mean semi-major axis that is constrained.

As an example, consider how many RSs we expect to observe around M67 at a given time due to triple disintegrations coming from single-binary interactions in the cluster core. Specifically, consider a circular field of view of radius 150 pc at the distance of M67. Moving at a tangential velocity of 30 km s^{-1}, a star will cross this field-of-view in roughly 10 Myr. But the time between single-binary interactions in M67 is $\lesssim$ 5 Myr (using the same parameters as adopted in Section 3.1 of Leigh and Geller (2013) but assuming a mean orbital separation of 100 AU instead, which is approaching the hard-soft boundary). Assuming all of these interactions resulted in the ejection of the decay products (i.e., binary and star for a single-binary interaction) at 30 km s^{-1} the cluster (which is roughly an order of magnitude higher than expected for the typical recoil velocity), we therefore expect an order of 2 RS/RB pairs from the cluster in this field of view at the present time due solely to single-binary interactions. If we observe more/less than this, this could imply that some of our assumptions are incorrect such as, for example, the mean binary orbital separation and/or the binary fraction. With that said, however, we expect few RS/RB pairs coming from individual clusters, but this lack of statistics can be somewhat mitigated by looking to other clusters as well.

To summarize this section, given the additional constraints available when searching for RS candidates coming from the triple disintegration scenario, the confidence level with which the RS candidate can be associated with a host cluster should be much higher than for the SN-induced mechanism. This is especially true when working without radial velocities and hence only five dimensions in phase space (i.e., three position parameters and two in velocity). In addition, it should be possible to distinguish RSs coming from each mechanism, given the discussed differences in their predicted properties, despite overlap in the predicted velocity distributions.

Chapter 3

Methodology

We develop a methodology to identify RS candidates from clusters coming from the disintegration of three-body systems formed from single-binary interactions, which we apply to the old OC M67 as a case study. To this end, we present our methodology for identifying not only interesting RSs, but also candidate RBs that are consistent with having interacted with them. The methodology results in a (short) list of RS/RB pair candidates and their corresponding observed properties.

3.1 Data acquisition

In this section, we introduce the data used to search for RS/RB pairs in the vicinity of M67, as well as our preliminary cuts in distance and position on the sky (but defer more in-depth calculations to an appendix A1).

3.1.1 Gaia DR3 Data

Ideally, we must build a 6-D phase space, requiring right ascension, declination, proper motions, radial velocity and parallax (i.e. distance). In our case, we are able to construct a nearly complete 5-D phase space using the Gaia DR3 catalog, but lack reliable radial velocities (see Section 5 for more of a discussion on the difficulties, or lack thereof, imposed on our analysis by lacking the sixth dimension). This data release represents a major advance with respect to Gaia DR2 and Gaia EDR3 because of the unprecedented quantity, quality, and variety of source astrophysical data. To date this is the largest collection

of all-sky spectrophotometry, radial velocities, variables, and astrophysical parameters derived from both low- and high-resolution spectra and includes a spectrophotometric and dynamical survey of SSOs of the highest accuracy (Gaia Collaboration et al., 2022). The photometry also features increased precision, but above all much better homogeneity across colour, magnitude, and celestial position. (Salomon et al., 2020; Gaia Collaboration et al., 2021; Brown et al., 2021). Even though Gaia DR3 includes the sixth data release from the Radial Velocity Experiment (RAVE) survey (Steinmetz et al., 2020), we do not include these data in our analysis. Excluding radial velocities quantifies how constraining are the data without the third dimension in velocity, which can be exceedingly difficult to obtain in many clusters (e.g., crowded fields). It is also important to note that the Gaia data require care when estimating distances from parallaxes that are either large ($\gtrsim$ 1 kpc) or have large uncertainties (Luri et al., 2018). Hence, we adopt a course-grained cut on distance for our candidates, as described in the subsequent section.

3.1.2 Preliminary sample selection

In order to identify our initial sample of candidate RSs, we extract from the Gaia data (Gaia Collaboration et al., 2022) a complete 5-D kinematic data set (i.e., proper motions, parallax and position on the sky) that covers our chosen field of view of $\sim$ 10 degrees radius on the sky or 150 pc radius from the centre-of-mass of M67 (i.e., forming a circular field of view in 2-D). This limit and hence our first cut in the data is decided, as calculated in Section 2, based on the calculated time between single-binary interactions and the expected ejection velocity from the cluster, such that of order unity RS/RB pairs are expected to be observed within our chosen field of view at any given time.

First, we apply a cut in distance. For this, we adopt a cylindrical volume with a radius of 150 pc and a length of 300 pc (in the direction of the cluster), centered on M67. We select all sources that lie within this 3-D cylinder. We do not use the uncertainties in parallax for this preliminary cut, which can be substantial in some cases (but see below).

Within this cylinder, we identify in total 203,190 objects not factoring in the uncertainties in parallax, whereas including objects with parallax uncertainties that make them consistent with lying within the domain of our cylinder to within

1-σ increases this number by about a factor of two. We do not include these additional objects in our initial sample since most of them are dim with large uncertainties in most of our 5-D parameter space. Hence, the inclusion of these additional objects will most likely not result in a significant change in our final sample of high probability or "best" candidate pairs. We note as well that the change in sample size we obtain upon performing a similar cut in the 2-D position on the sky (i.e., including all sources that lie within 1-σ of falling inside our circular field of view) is negligible given the small uncertainties. Hence, we also do not include these additional objects in our initial sample.

For our second cut in the data, we do not consider objects located within the cluster in projection on the plane of the sky. Using for the cluster center $\alpha = 8^h51^m23^s.3$, $\beta = +11°49'02"$ (J2000) (Jacobson et al., 2011), we identify those RSs located outside the cluster tidal radius. In previous studies, the tidal radius was found to be either 14 ± 2.5 pc (Keenan et al., 1973), 16.8 pc (Davenport and Sandquist, 2010) or 17.98 pc (Kharchenko et al., 2013). For simplicity and to choose a balance between these values, we adopt a tidal radius of 17 pc. For all of our calculations, we assume the following additional parameters for M67. We assume a total mass of the cluster $M_{cl} = 2100 \pm 600$ $M_\odot$, core radius $r_c = 1$ pc (Bonatto, Ch. and Bica, E., 2003) and a half light radius $r_h = 2.6$ pc (Balaguer Núñez, 2006).

Finally, we remove from our sample all objects with 2-D velocities smaller than the escape velocity from M67 relative to the cluster centre of mass. For this, we adopt an escape velocity of 2.6 km/s, calculated using the method adopted in Georgiev et al. (2009) by assuming a correction factor of $f_{c,t}(1.2) = 0.09154$ (corresponding to the velocity once the object reaches the tidal radius). We also consider only sources that the velocity vector points opposite to the tidal radius. This cut reduces our sample size from 203,190 to 15,346 sources.

3.2 Final sample selection

In this section, we apply the cuts to our data described in Section 2, which are applied to identify the most likely candidate RS/RB pairs that were ejected from M67 due to single-binary interactions. We begin, as described in the previous section, with a total of 15,346 objects, yielding in total 235,499,716 possible pairs. If we then eliminate all duplicate pairs, this leaves us with a sample size of 117,864,981.

3.2.1 Traceback position and time

First, we identify every pair of objects whose 2-D velocity vectors trace back to intersect within the tidal radius of M67. This is done as follows. Using equation **A1**, we first transform to a coordinate system in velocity-space that is centered on the centre-of-mass motion of M67. We then calculate in this frame the 2-D proper motion vector for every object in both magnitude and direction using the Gaia proper motions in both RA and Dec (van Leeuwen, 2009, Gaia Collaboration et al., 2018, Getman et al., 2019, and Kuhn et al., 2019, see eq. A2, A3 and A4), along with the corresponding uncertainties.

Using the proper motions and their uncertainties in RA and Dec, we calculate three vectors for each object, yielding three limiting angles of intersection given by equations A1.10, A1.11 and A1.12. We then calculate three points of intersection, called cross-points, by applying the equations in Section A1.3

We keep in our sample all pairs with at least one of these three limiting cross-points lying within the tidal radius of M67, and discard the rest.

Next, all pairs of candidate objects with cross-points located within the domain of M67 must coincide in not only space but also time. Hence, we calculate for both objects in every pair the traceback time (TBT) to the location of the cross-point, defined as the time taken to travel from the cross-point to the presently observed object position. This is done using the measured values in both distance traveled and velocity, assuming the presently observed velocity is constant and has not changed over the extent of its travel across the field of view. We then calculate an uncertainty by propagating the provided uncertainties in both position and velocity. Hence, the time it will take object a (and it is the same for object b) to

reach the cross-point is given by:

$$TBT_{\rm a} = \frac{|\vec{r}_{\rm a} - \vec{r}_{\rm cp}|}{|\vec{v}_{\rm a}|} = \sqrt{\frac{\left(r^{\rm x}_{\rm a} - r^{\rm x}_{\rm cp}\right)^2 + \left(r^{\rm y}_{\rm a} - r^{\rm y}_{\rm cp}\right)^2}{\left(v^{\rm x}_{\rm a}\right)^2 + \left(v^{\rm y}_{\rm a}\right)^2}} \tag{3.2.1}$$

$$TBT_{\rm b} = \frac{|\vec{r}_{\rm b} - \vec{r}_{\rm cp}|}{|\vec{v}_{\rm b}|} = \sqrt{\frac{\left(r^{\rm x}_{\rm b} - r^{\rm x}_{\rm cp}\right)^2 + \left(r^{\rm y}_{\rm b} - r^{\rm y}_{\rm cp}\right)^2}{\left(v^{\rm x}_{\rm b}\right)^2 + \left(v^{\rm y}_{\rm b}\right)^2}} \tag{3.2.2}$$

where $\vec{r_{\rm a}}$ is the distance separating the object's current position from the centre-of-mass of M67 and $\vec{v_{\rm a}}$ is the velocity relative to the centre-of-mass motion of M67. Similarly, $\vec{r}_{\rm cp}$ is the vector from the centre-of-mass of M67 to the cross-point with $r^{\rm x}_{\rm cp}$ and $r^{\rm y}_{\rm cp}$ being the corresponding values for each coordinate. If the difference in TBT values for a given pair of objects is consistent with zero to within 1-σ, we keep the pair in our sample and discard it otherwise.

3.2.2 Angle of intersection between velocity vectors

We further require that, in the plane of the sky, the angle between their velocity vectors (to the hypothetical cross-point) of a given pair must be consistent with 180°, as illustrated in Figure 3.2.1. To evaluate this consistency, we use the two limiting vectors described above when evaluating the possible range of cross-points for each pair, which yield a minimum (lower) and maximum (upper) possible angle (using the 1σ uncertainties in both directions). We calculate the angle between the intersection of each pair of vectors using eqs. A1.10, A1.11 and A1.12. If a given pair has an angle of intersection consistent with 180° to within these upper and lower bounds, we keep it in our sample and discard it otherwise.

3.2.3 Velocity ratio

We also require that both objects should have velocities consistent with linear momentum conservation. This means that, assuming that the slower moving object is a binary at least twice as massive as its single star counterpart (and hence that it was the lowest mass star that was ejected from the three-body interaction

as a single), the ratio of object velocities should exceed two. We apply this cut to our data using the provided proper motions in RA and Dec by calculating a total magnitude for each object velocity in 2-D (relative to the centre-of-mass motion of M67), and then use these values to compute a ratio. We propagate the 1-σ uncertainties in proper motions to compute an uncertainty for each velocity ratio. We then keep in our sample all pairs that have a velocity ratio greater than two by 1-σ or more and discard them otherwise (but see below for including with this velocity ratio cut the requirement that the slower moving object should likely be more massive and hence brighter).

3.2.4 Position in the colour-magnitude diagram of the progenitor cluster

Finally, we assess whether or not both objects in each pair have a location in the CMD that is consistent with having originated from M67 using the g_{bp} and g_{rp} filters. Specifically, we require than one object (the candidate single star) should lie within 1-σ of an isochrone for M67 in both colour and brightness simultaneously (but note that our results do not change significantly if we instead use both magnitudes instead of a colour), while the other object (the candidate binary) should lie within 1-σ (in both colour and brightness) of the area in colour-brightness-space defined as the region between the isochrone and an identical track shifted upward by 0.75 mag (corresponding to the equal-mass binary sequence). Additionally, it is the slower object that should be the brighter one from linear momentum conservation (assuming the brighter object is more massive). To evaluate this, we use the PARSEC isochrone fit provided in Childs et al. (2023). We consider that the pair is a valid candidate if the dimmest object is the fastest and it simultaneously lies within 1-σ of the isochrone in both magnitude and colour. At the same time, the slower object must be consistent with lying between the isochrone and the equal-mass binary sequence to within 1-σ in both magnitude and colour. If both objects in a given pair satisfy this criterion then we keep it in our sample and discard it otherwise.

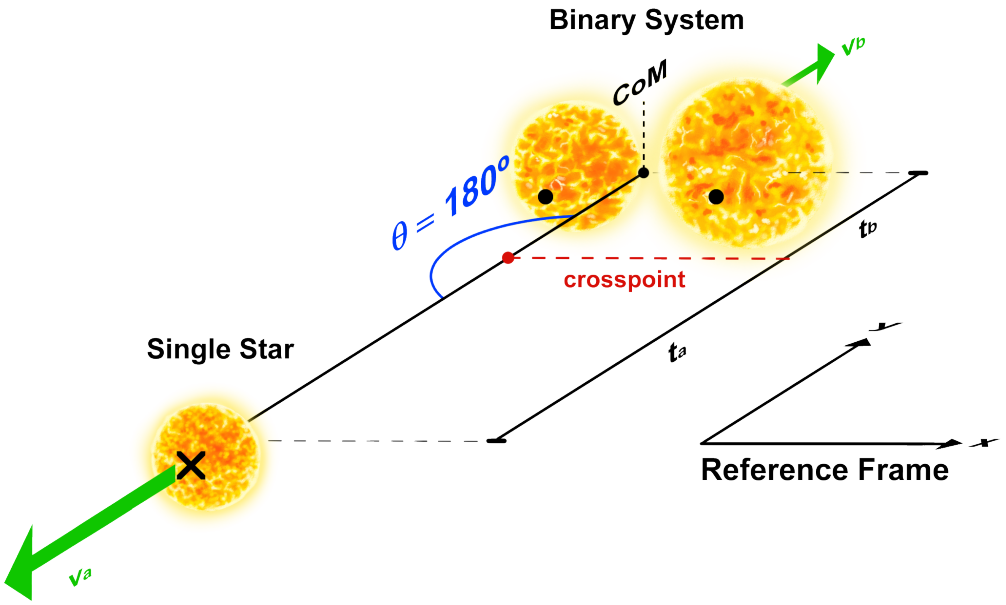

Figure 3.2.1: Diagram illustrating the key criteria used to identify sources that have interacted in a three-body system, including the cross-point, angle, and traceback time. Direction and velocity vectors for both single runaway ($v_{\rm a}$) and binary runaway ($v_{\rm b}$) sources are indicated. The centre-of-mass of the binary system (indicated with an "CoM") is given as a reference point. The time it takes for the single source to reach the crosspoint ($t_{\rm a}$) and for the binary source ($t_{\rm b}$) are also indicated.

Chapter 4

Results

In this chapter, we first describe the results of our analysis, focusing on the fraction or number of pairs that simultaneously satisfy all of the criteria described in the previous section. Our initial preliminary sample size, described in Section 3.1.2, is 117,742,185. We present our most probable candidate RS/RB pairs, indicating for each how well they satisfy each criterion.

4.1 Final sample

In this section we describe in brief to what degree our initial sample satisfies each of our adopted selection criteria. We quantify how strict is each of the criteria adopted to filter the initial number of pairs.

4.1.1 Traceback position and time distributions

The first cut applied to the data is one that ensures that the velocity vectors of a given pair of objects, rewound back in time, intersect in 2-D space at some point that is consistent with lying within the tidal radius of M67. Second, we require that these traceback vectors intersect not only in space but also time. These cuts reduce our initial sample size by, respectively, 56% and 90%. The distributions in both the ratio and difference in traceback times for each pair are shown in Figure 4.1.1.

The reason for the fact that these cuts only reduce our sample size by roughly an order of magnitude is that most objects have velocities that follow an overall

Galactic flow, and hence tend to point in similar directions with comparable magnitudes. Additionally, all objects lie a roughly similar distance away from the centre-of-mass of M67 (i.e., to within a factor of a few given our field of view and the limiting tidal radius of M67). Given these limitations, it is not so surprising that a relatively large fraction of pairs are consistent with having originated from M67 while also having similar traceback times.

4.1.2 Distribution of angles of intersection between velocity vectors

We further require that a given pair have an angle at the cross-point between the two velocity vectors that is consistent with 180°, as predicted from linear momentum conservation. To this end, we compute the angle of intersection for every pair of objects in our sample. The resulting distribution is shown in Figure 4.1.2.

As is clear, the least probable angle to obtain is 180°, making this cut especially constraining. The typical uncertainty in this angle is highly dependent on how dim the two objects in a given pair are, but is around a degree for pairs having both members brighter than $G_{bp} < 20$. Hence, most sources do not fall within 1-σ of 180°. Specifically, this cut reduces our initial sample size by 99%.

It is however worth noting that part of the reason for the low probability associated with an angle of 180° is that, as already described, most stars follow an overall "Galactic flow", such that their velocity vectors tend to be more aligned than not, and with similar magnitudes.

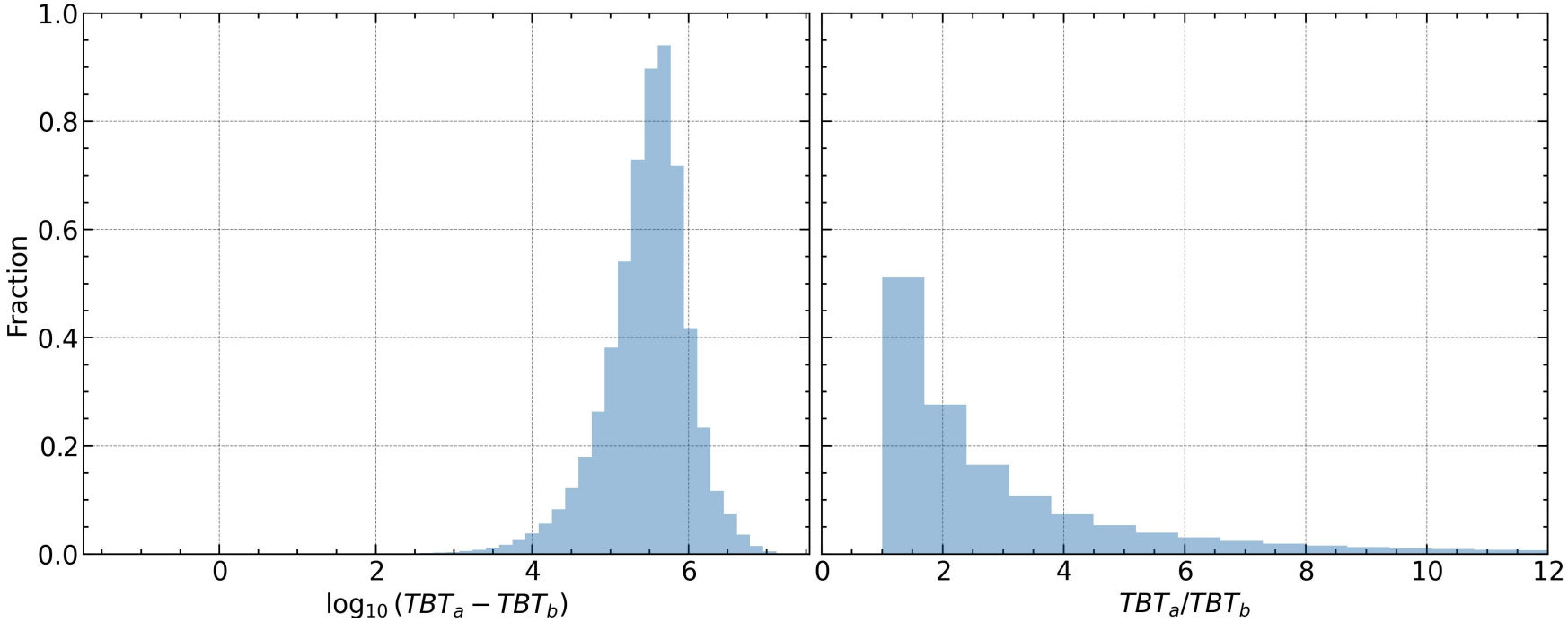

Figure 4.1.1: Histograms showing the distribution of the difference in traceback times (left inset) as well as their ratio (right inset) for every pair in our sample. The TBTs are provided in years.

4.1.3 Velocity ratio distribution

In order to keep a given pair in our sample, we require that the velocity ratio of a given pair exceed two by at least 1-σ. The distribution of velocity ratios for every pair in our sample is shown in Figure 4.1.3, where the velocities are computed with respect to the cluster centre-of-mass motion. The vertical dashed line indicates the critical velocity ratio of two. As is clear, this cut is not especially constraining for the same reasons discussed in the previous sections (i.e., most objects seem to follow an overall Galactic flow). It reduces our initial sample size by 67%.

Finally, since we have assumed that it is always the least massive object ejected from a three-body interaction, we also require that for each pair the slower moving object should be the brighter one. If we apply this simple cut after the one made previously in this section, we further reduce our sample size by one order of magnitude in total from the initial sample.

4.1.4 Position in the colour-magnitude diagram

Both objects should lie within 1-σ (simultaneously in both colour and brightness) of the area in colour-brightness-space defined by the region between the isochrone and an identical track shifted upward by 0.75 mag (corresponding to the equal-mass binary sequence). Finally, we require that for a given pair, the fastest source (the candidate single) must lie within 1-σ (in both colour and brightness) of an isochrone for the progenitor cluster. By applying the criteria that the dimmest object must be the fastest and the slowest object must be the brightest, we reduce the total sample by 56%. Further, considering the fact that the fastest star lies within the isochrone with 1σ confidence, we eliminate approximately 98.5% of the total sample.

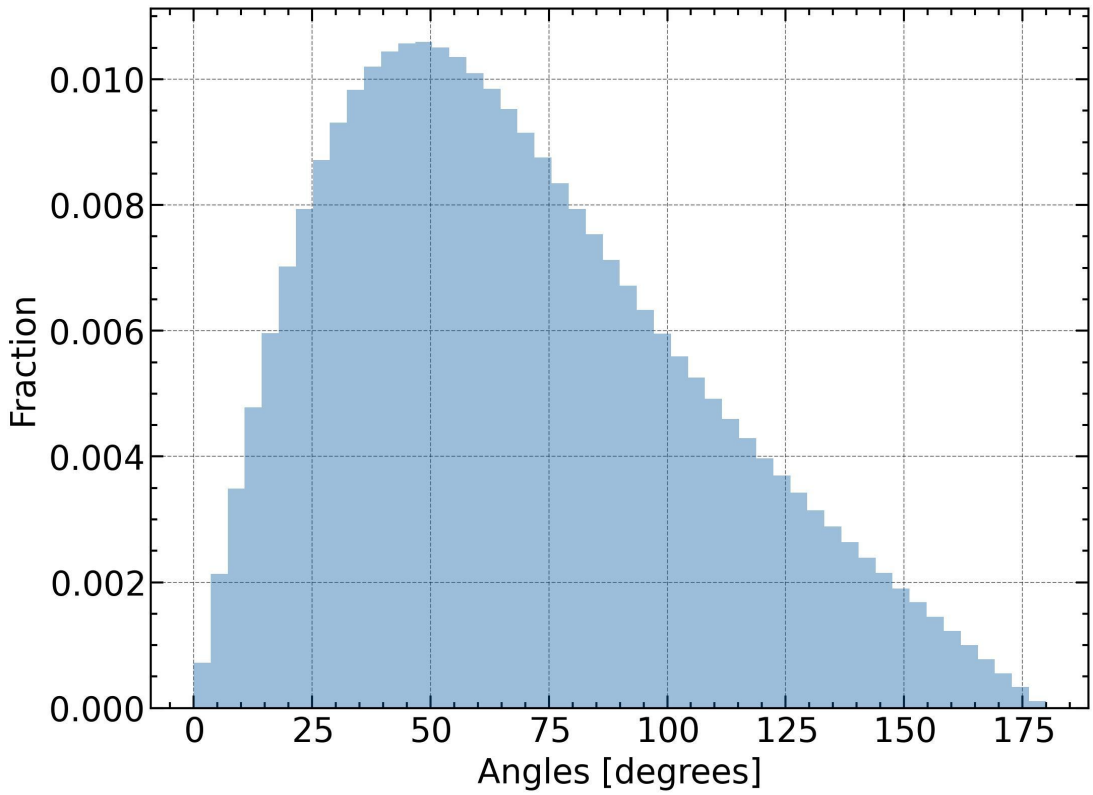

Figure 4.1.2: Histogram showing the distribution of intersection angles between the velocity vectors for every pair in our sample. The x-axis shows the angle in degrees.

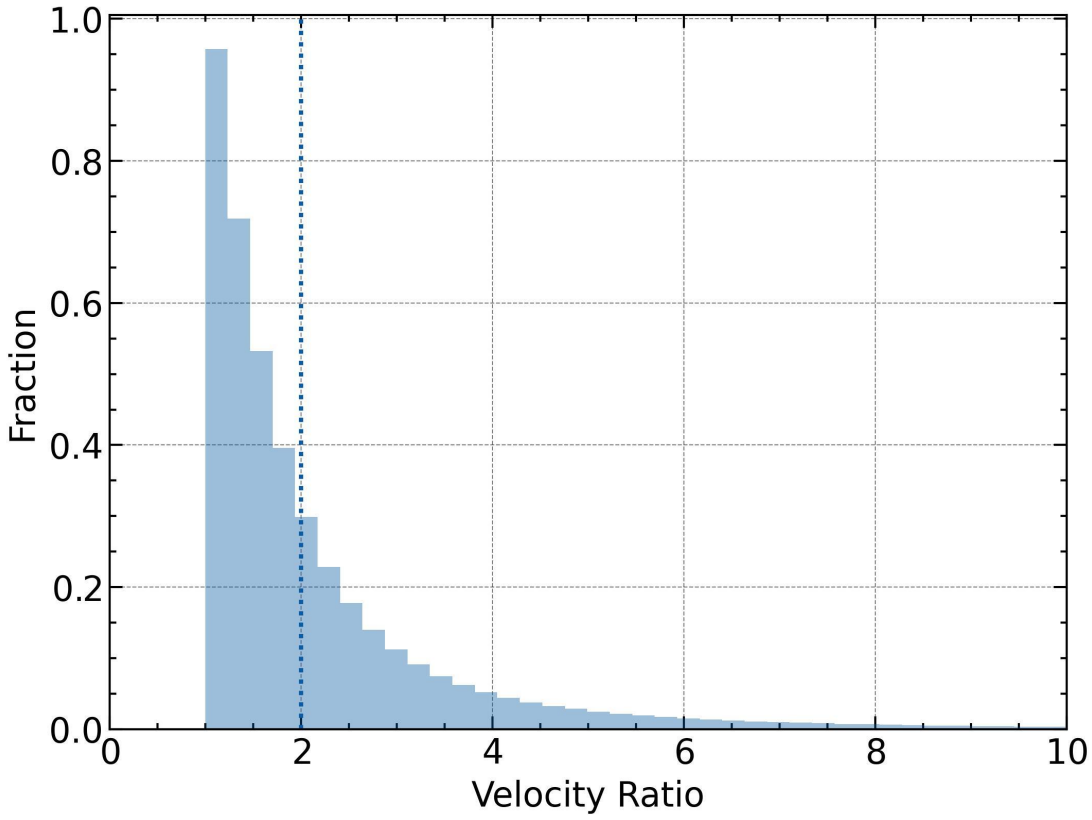

Figure 4.1.3: Histogram showing the distribution of velocity ratios for every pair in our sample. The vertical dashed line shows a critical ratio of two, and it is only above this line that we expect to associate binary runaways with their single counterparts.

4.2 How many candidates are left?

After applying all of the above criteria, we are left with only one pair that satisfies them all simultaneously. This one pair is shown in Figure 4.2.1. The small dots show cluster members obtained from Childs et al. (2023), whereas the two large circles correspond to the two components of our one candidate pair. The lines show an isochrone fit and the equal-mass binary sequence (obtained by shifting the isochrone up in brightness by 0.75 mag). The colour-coding indicated in the provided legend shows which of the two objects is the fastest, confirming that it is indeed the brighter object that is moving slower.

Therefore, after applying all of the criteria available to us from momentum conservation and causality, our total sample size is reduced by eight orders of magnitude, from $\sim 10^8$ to 1.

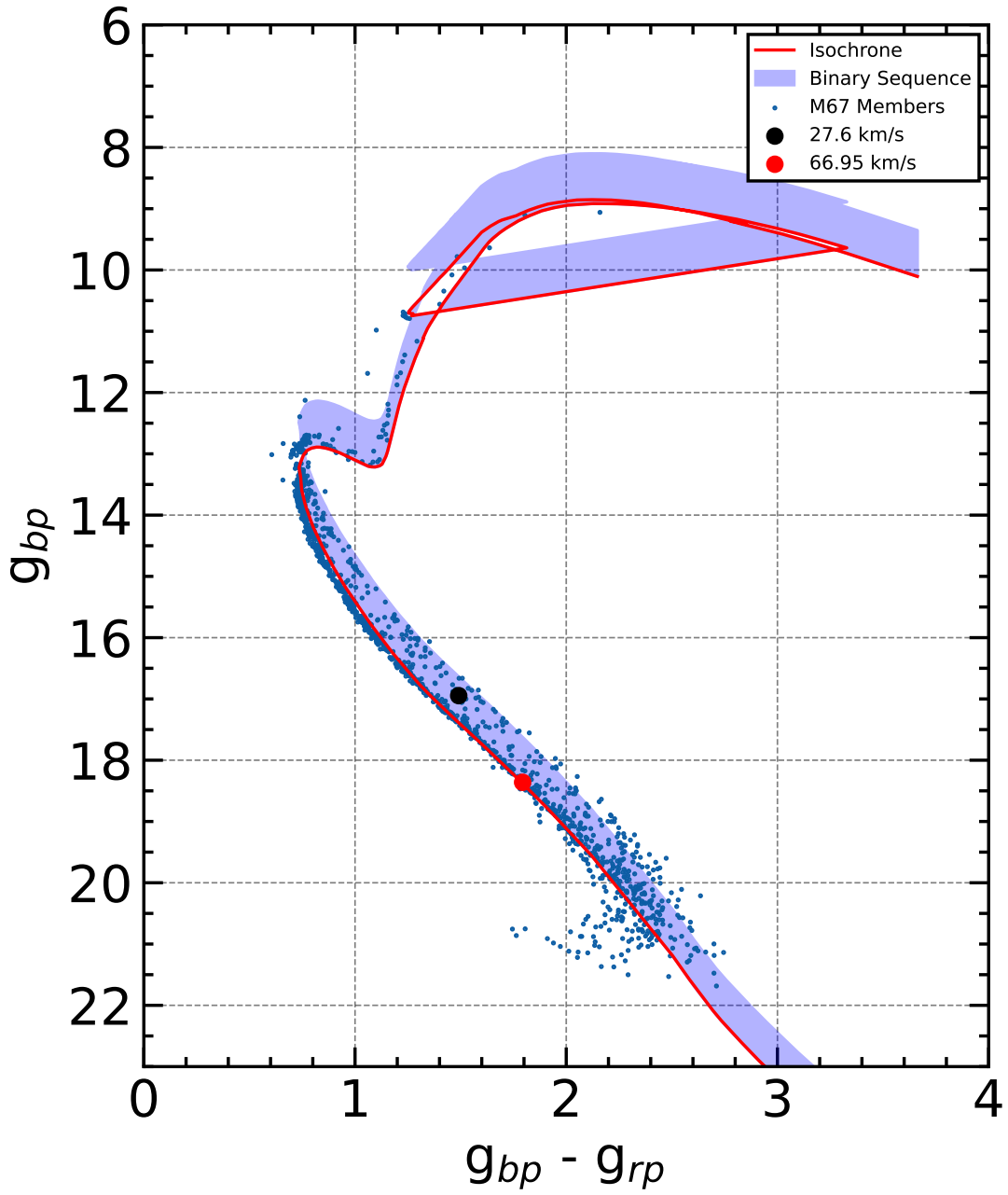

Figure 4.2.1: Colour-magnitude diagram of the old open cluster M67 plotted using the Gaia data, selecting only those stars indicated as high-probability cluster members in Childs et al. (2023), plotted as small blue dots (note that this catalog excludes objects that do not fall on an isochrone, removing objects such as blue stragglers). The solid red lines show the best-fitting isochrone (lower line) as well as the equal-mass binary sequence shifted 0.75 mag above it (upper line). The larger dots indicate the two components of our one candidate pair that passes all of our criteria. The red and black dots correspond to, respectively, the faster and slower moving objects. The cluster members do not include blue stragglers and other binary evolution products because they are far from a standard isochrone fit.

4.3 Catalog

In this section, we present a catalog of our 10 most probable RS/RB pairs. That is, we provide the properties of those pairs that satisfy the largest number of our selection criteria. Although the choice is arbitrary, we chose 10 pairs since this provides a basis for comparison, and a reasonable balance between length and a rough "probability" of actually being a legitimate ejected RS/RB pair. We caution, however, that there is no a priori reason why satisfying the largest number of our criteria should indicate the highest probability pairs, and taking this approach could exclude actual RS/RB pairs that were ejected from the cluster. With that said, however, we do notice that beyond roughly 10 candidates those objects that satisfy our criteria tend to do so because they have large uncertainties.

Our final catalog is provided in Table 4.3.1, which gives observed and calculated quantities for each pair along with the corresponding 1-σ uncertainties. Each row corresponds to a different candidate pair. In the first two columns, we provide the object IDs from the Gaia data for each component of a given pair, labeled as object a and object b, where object a has the larger velocity. Columns 3 and 4 give for object a and b the magnitude corresponding to the blue Gaia passband, respectively, whereas columns 5 and 6 show the same thing but for the red passband. Columns 7 and 8 provide the velocity in km s^{-1} and the corresponding 1-σ uncertainty. Column 9 answers the question: Is the brighter object traveling slower. Column 10 is the velocity ratio between both sources and the respective 1-σ uncertainty. Column 11 provide the difference in TBTs and the corresponding 1-σ. Columns 12 give the angle of intersection along with, respectively with 1-σ. Columns 13 answers the question: Do the fastest objects in the pair satisfy our CMD constraints derived from the isochrone fit?

Table 4.3.1 illustrates an important trend in the data. That is, we observe a tendency for dim objects to have larger proper motion (and magnitude) uncertainties, which translates into larger uncertainties for the calculated angles of intersection, traceback times and velocity ratios. Hence, our selection criteria become more constraining with increasing object brightness.

Table 4.3.1: Best 10 resulting pairs

	ID_a (Gaia DR3)	ID_b (Gaia DR3)	$g_{bp,a}$	$g_{bp,b}$	$g_{rp,a}$	$g_{rp,b}$	v_a [km/s]	v_b [km/s]	Brighter = Slower?	v_{ratio}	TBT_{diff} [Myr]	$\theta_{a,b}$ [degree]	Isochrone Fit?
1	599619181604349440	604856670884640384	18.36	16.95	16.57	15.46	66.9+/-0.4	27.60+/-0.24	YES	2.426+/-0.026	0.005+/-0.007	179.6+/-0.5	YES
2	599610561605532928	604856670884640384	16.97	16.95	15.49	15.46	84.38+/-0.26	27.60+/-0.24	YES	3.057+/-0.029	0.006+/-0.006	179.6+/-0.5	NO
3	662118862798733824	591491424147901184	19.52	15.92	17.12	14.79	70.8+/-2.3	35.36+/-0.16	YES	2.00+/-0.07	0.001+/-0.027	178.5+/-1.8	NO
4	648620154247150080	604513730630053504	21.21	20.99	18.57	18.41	64.3+/-3.0	29.2+/-1.5	YES	2.20+/-0.15	0.00+/-0.06	179.1+/-2.8	NO
5	648804081926315904	604207237468507264	21.34	20.64	18.71	18.16	50.1+/-2.7	23.6+/-1.4	YES	2.13+/-0.17	0.05+/-0.08	178+/-4	NO
6	3146483729561664000	606054623161267072	21.29	21.01	18.69	18.53	30.4+/-1.8	12.4+/-1.8	YES	2.5+/-0.4	0.18+/-0.23	173+/-8	NO
7	3093040111468262400	608838414804007168	21.13	20.03	18.58	17.41	21.4+/-1.9	3.0+/-0.9	YES	7.0+/-2.1	0.1+/-0.5	165+/-21	NO
8	601160838641459072	605806653225091840	17.85	18.28	16.04	16.43	57.6+/-0.5	27.9+/-0.4	NO	2.06+/-0.04	0.014+/-0.015	179.7+/-0.9	NO
9	636701005819917440	596194237243454976	16.97	20.69	15.57	18.02	37.78+/-0.28	18.2+/-1.1	NO	2.08+/-0.13	0.01+/-0.07	179+/-4	NO
10	3097964789688276736	604221123098059776	19.92	20.54	17.64	18.14	40.3+/-0.8	17.0+/-2.9	NO	2.4+/-0.4	0.03+/-0.18	175+/-9	NO

** Although the choice is arbitrary, we chose 10 pairs since this provides a basis for comparison, and a reasonable balance between length and a rough "probability" of actually being a legitimate ejected RS/RB pair. We caution, however, that there is no a priori reason why satisfying the largest number of our criteria should indicate the highest probability pairs, and taking this approach could exclude actual RS/RB pairs that were ejected from the cluster.*

Chapter 5

Discussion

In this chapter, we discuss possible caveats of our methodology as well as possible improvements on it in future work.

5.1 False positives

How many false positives do we expect from our analysis? Said another way, if we choose a random position on the sky, how many pairs in a field of view comparable to the one assumed herein do we expect to simultaneously satisfy all of our selection criteria? To address this, we choose a position on the sky shifted in either RA or Dec by 150 pc and then repeat our analysis for all pairs in this field of view. This generates four different tests corresponding to the four different RA/Dec combinations (i.e., positive/negative shift in RA and/or a positive/negative shift in Dec). In total, this generates an initial sample of 468,586,715 pairs that we apply our methodology to, which is four times greater than the initial sample size we obtain. Out of all these pairs, zero objects satisfy all of our criteria simultaneously (mostly due to the CMD location requirements).

In general, based on this analysis, we expect the frequency of false positive detection to be lower than 10^{-8}, and hence lower than the detection frequency found in this investigation (i.e., 1 out of 10^8). The most likely false positives should in general be associated with dimmer objects, due to the larger uncertainties.

With that said, the methodology presented exploits the causality and conservation of momentum expected for triple disintegrations, making runaways produced from

this mechanism potentially more reliably identifiable than runaways produced from other mechanisms, such as in young star clusters where runaways are expected to be produced from supernovae explosions in binaries at a non-negligible rate. Consider for comparison how many false positives we would have obtained had we been looking for runaways produced from SN explosions in binaries. Here, our primary constraints are checking to see if both the velocity vectors as well as the location in the progenitor cluster CMD of a candidate runaway are consistent with having originated from a progenitor cluster. Starting with the initial sample derived in Section 3.1.2, these two cuts together reduce the sample size by 98%. This reduction is still much smaller than the total reduction in sample size for the triple disintegration mechanism. Specifically, we would end up with a final sample three orders of magnitude larger than for the triple disruption scenario. This makes for the SN scenario approach at looking for runaways untractable, at least in old star clusters where associating the runaway with a SN remnant in the progenitor cluster is highly unlikely.

5.2 The effects of the Galactic potential

Our method neglects the effects of the Galactic potential. This is because the expectation is that any changes imparted to the velocity vectors of escapers from M67 should be small over our chosen field of view. This assumption turns out to be a good approximation when both objects in a given pair have high velocities and are located close to the cluster, such that their travel times to their currently observed locations is short. However, this assumption can fail substantially when the object velocities are low and their positions are far from the host cluster. This is illustrated in Figure 5.2.1.

Figure 5.2.1 shows the results of simulating 500 ejection events from M67. For each, the trajectories of the ejected objects are integrated in the Galactic potential using AMUSE (Astrophysical Multipurpose Software Environment, Pelupessy et al., 2013) a component library for performing astrophysical simulations involving different physical domains and scales and galpy: A Python Library for Galactic Dynamics (Bovy, 2015). We work with over a 50 pc distance (i.e., a distance representative of that for our identified candidate pair) from the centre-of-mass of the progenitor cluster (for the single star only), and the final angle between their

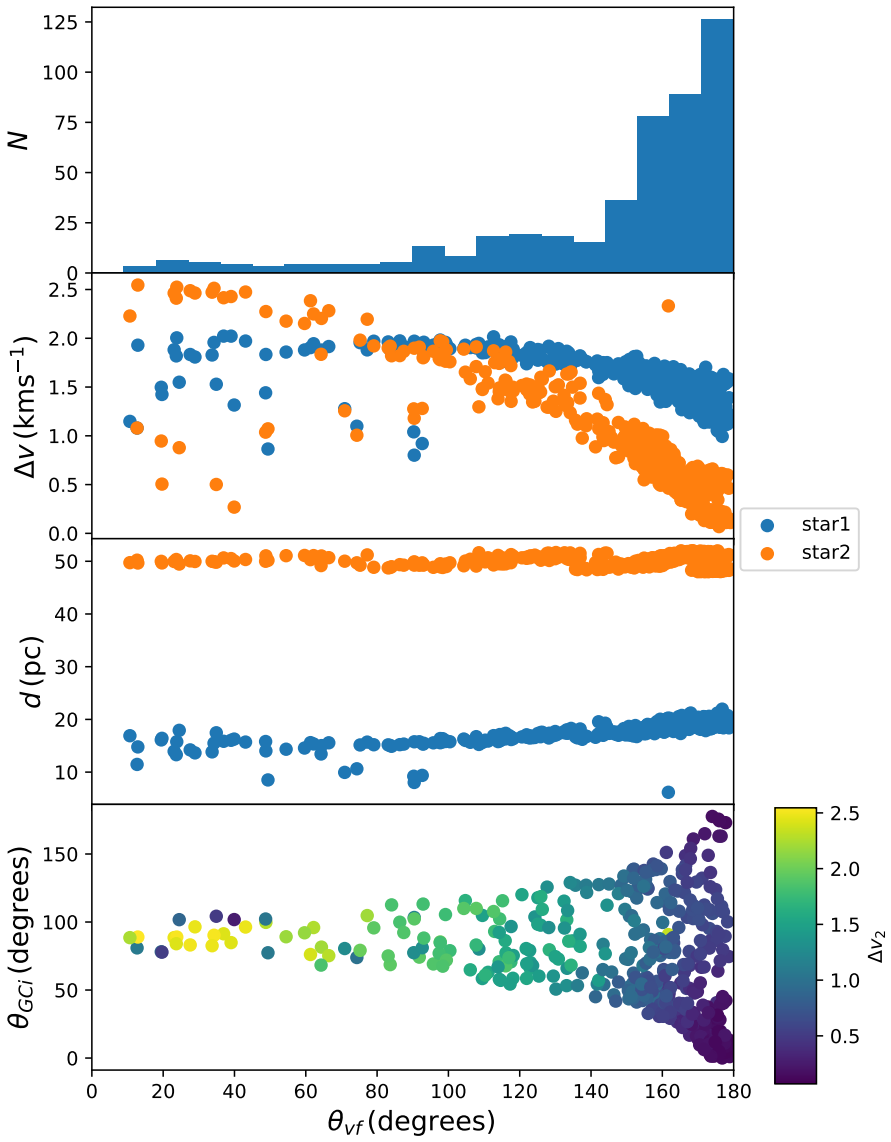

Figure 5.2.1: The results of integrating the trajectories of escapers from M67 in the Galactic potential until the least massive object reaches 50 pc from the cluster centre. Each inset is plotted with respect to the final angle between the 3-D velocity vectors of the escapers, θ_{vf}. (The initial angle between the velocity vectors is 180°). The top panel shows a histogram of the distribution of θ_{vf} for all pairs. The second panel from the top shows the total change in velocity magnitude for each object in each pair. The third panel from the top shows the final distances from the cluster center. In both the second and third panels from the top, blue dots correspond to the binary, and orange dots correspond to the single star. In the bottom inset, the y-axis shows the initial direction of ejection of the lighter star, where $\theta_{GC} = 0$ corresponds to ejection directly toward the Galactic Centre, and $\theta_G C = 90°$ corresponds to ejection along the plane perpendicular to the galactic plane (the intersection of these planes includes the direction of motion of the orbiting cluster). In this panel, the data points are colour-coded by the total change in velocity of the lighter ejected object (i.e., the single star)

velocity vectors as well as the change in magnitude of the velocities are calculated. The initial velocity of the binary is set equal to the cluster escape velocity, and the initial single star speed is then decided assuming linear momentum conservation. Hence, we adopt the minimum possible ejection velocity, which maximizes the effects of the Galactic potential in changing the object velocities over our chosen field of view. We note that we work with 3-D velocities, but these results remain unchanged using 2-D velocities.

As indicated by the colour-coding the bottom panel of Figure 5.2.1, most pairs experience the most significant change in velocity when ejected parallel to the orbital motion of the cluster and the smallest change in velocity when ejected perpendicular to it. Note as well that objects tend to be decelerated in the former case and accelerated in the latter. As is clear, for those objects leaving the cluster with small escape speeds, it is indeed possible for the final angle of intersection between their velocity vectors to deviate significantly from 180°. This becomes even worse if a larger field of view is considered, and the orbits are integrated out to 150 pc or more.

Importantly, if we instead adopt for the initial binary velocity ten times the cluster escape speed, then Figure 5.2.1 changes dramatically, and 100% of the pairs have a final intersection angle within 5° of 180°. We note that this is roughly the case for the one candidate pair identified in this investigation, since the observed velocities are of order a factor of ten larger than the cluster escape speed, and both objects are close to M67 in projection on the sky. Nevertheless, the results of this preliminary analysis suggests that the effects of the Galactic potential should be considered in future work when searching for ejected RS/RB pairs from clusters, but should be minimized for faster objects located closer to the progenitor cluster.

5.3 The sixth dimension

In order to further validate our method and confirm or refute the pair of RS/RB candidates identified here, radial-velocity follow-up observations can be used. This can not only constrain whether or not a given pair is consistent with having originated from the progenitor cluster along the line-of-sight, but also potentially the binary nature of the RB candidate and even its orbital properties. Although our candidate pair is relatively bright relative to most stars in the cluster, it

should be regarded with caution given that our analysis lacks the sixth dimension. This makes additional predictions based on momentum conservation and causality that can be tested using radial velocity measurements (to confirm/reject that it is consistent with having originated from M67 and confirm/reject that it is a binary).

Chapter 6

Conclusion

In this thesis, we present a systematic methodology to identify runaway stars ejected from star clusters due to single-binary interactions. This is done by exploiting the fact that we expect such disintegrations to produce a pair of objects, namely a single star and a binary, with their relative velocity vectors, positions on the sky and positions in the progenitor cluster CMD being consistent with linear momentum conservation and causality (i.e., both objects are consistent with having originated from within the cluster at the same time). Using the old open cluster M67 as a benchmark test case, we confront our presented theoretical expectations with a 5-D kinematic data set obtained from the Gaia EDR3 catalog, using the provided parallaxes, proper motions and positions on the sky.

Our analysis yields, out of an initial sample size of roughly 10^8 candidate pairs, only one single/binary pair that simultaneously satisfies all of our selection criteria. We present the distributions of calculated quantities for our entire sample to illustrate which of our criteria are the most constraining, as well as the calculated properties of our 10 best candidate pairs (i.e., those that simultaneously satisfy the largest number of our selection criteria). We find that a small fraction ($< 1\%$) of our initial sample of candidate pairs have an angle of intersection between their velocity vectors that is consistent with 180° to within 1-σ. Additionally, of order 10% of our initial sample simultaneously have a ratio of velocities that exceeds two with the brighter of the two objects in the pair traveling the slowest. Both of these criteria are expected from linear momentum conservation, and tend to be more constraining than simple causality arguments related to the relative travel

times and distances of both objects in a given pair being commensurate.

The discovery of RS/RB pairs coming from M67, if confirmed, can in turn constrain both the progenitor cluster dynamical evolution and the underlying binary fraction and distributions of binary orbital properties. For example, their numbers and properties can be used to constrain the rate of single-binary interactions, as well as the approximate energetics of the interactions, by constraining the orbital separation of a typical binary in the cluster. This is because the mean rate of single-binary interactions scales linearly with the mean binary orbital separation in the limit that gravitational focusing dominates the overall collisional cross-section (e.g. Leigh and Sills, 2011). For M67, we find that a mean orbital separation of ~ 100 AU is consistent with of order unity ejected RS/RB pairs being observed within our chosen field of view, which is consistent with the number of RS/RB pairs that satisfy all of our selection criteria. Additionally, if the current orbital separation of a given RB can be measured then, assuming the kinetic energy of the interaction was roughly consistent with what is expected from the observed cluster velocity dispersion (i.e., again corresponding to a mean), energy conservation can be used to constrain the initial binary orbital separation, and in turn constrain the underlying distribution of binary orbital separations by, for example, addressing whether or not the observed RS/RB properties are anomalous or expected for a given assumed distribution of binary orbital separations.

While the results obtained in this study for M67 are promising, it is important to bear in mind that our candidate pair is still highly preliminary and should be further constrained using, for example, radial velocities and abundances. Also, it is important to validate our method by applying it to other star clusters. This would not only further test the effectiveness of our method but would also potentially provide valuable insight into the dynamical evolution of other clusters. Furthermore, by studying multiple clusters, we could potentially identify trends in the properties of RS/RB pairs and test current theoretical predictions for the internal dynamical evolution of the progenitor clusters. That is, our method can reveal differences in runaway demographics between different clusters, which would give valuable information on the dynamical evolution of different types of clusters. In future work, we hope to apply our method to a large sample of clusters to generate the required statistics to address these questions.

Bibliography

Andersson, E. P., Agertz, O., and Renaud, F. (2020). How runaway stars boost galactic outflows. *Monthly Notices of the Royal Astronomical Society*, 494(3):3328–3341.

Balaguer Núñez, M. D. (2006). *Astrophysical studies on open clusters: NGC 1807, NGC 1817, NGC 2548 and NGC 2682*. PhD thesis, University of Barcelona, Spain.

Balaguer-Nunez, L., Galadi-Enriquez, D., and Jordi, C. (2007). VizieR Online Data Catalog: NGC 2682 uvby-Hbeta photometry (Balaguer-Nunez+, 2007). *VizieR Online Data Catalog*, pages J/A+A/470/585.

Blaauw, A. (1961). On the origin of the O- and B-type stars with high velocities (the "run-away" stars), and some related problems. , 15:265.

Bonatto, Ch. and Bica, E. (2003). Mass segregation in m67 with 2mass. *AA*, 405(2):525–530.

Bovy, J. (2015). galpy: A python library for galactic dynamics. *The Astrophysical Journal Supplement Series*, 216(2):29.

Brown, A. G. A., Dekker, G., and de Zeeuw, P. T. (1997). Kinematic ages of OB associations. *Monthly Notices of the Royal Astronomical Society*, 285(3):479–492.

Brown, A. G. A., Vallenari, A., Prusti, T., de Bruijne, J. H. J., Babusiaux, C., Biermann, M., Creevey, O. L., Evans, D. W., Eyer, L., and et al. (2021). Gaia early data release 3. *Astronomy Astrophysics*, 650:C3.

Cantat-Gaudin, T., Jordi, C., Vallenari, A., Bragaglia, A., Balaguer-Núñez, L., Soubiran, C., Bossini, D., Moitinho, A., Castro-Ginard, A., Krone-Martins, A., Casamiquela, L., Sordo, R., and Carrera, R. (2018). A Gaia DR2 view of the open cluster population in the Milky Way. *Astronomy and Astrophysics*, 618:A93.

Carretero-Castrillo, M., Ribó, M., and Paredes, J. M. (2023). Galactic runaway o and be stars found using gaia dr3. *Astronomy amp; Astrophysics*, 679:A109.

Casamiquela, L., Castro-Ginard, A., Anders, F., and Soubiran, C. (2021). The (im)possibility of strong chemical tagging. *Astronomy amp; Astrophysics*, 654:A151.

Childs, A. C., Geller, A. M., von Hippel, T., Motherway, E., and Zwicker, C. (2023). Goodbye to Chi-by-Eye: A Bayesian Analysis of Photometric Binaries in Six Open Clusters. *arXiv e-prints*, page arXiv:2308.16282.

Colaboration, G., Helmi, A., van Leeuwen, F., McMillan, P. J., Massari, D., Antoja, T., Robin, A. C., Lindegren, L., Bastian, U., Arenou, F., Babusiaux, C., Biermann, M., Breddels, M. A., Hobbs, D., Jordi, C., Pancino, E., Reylé , C., Veljanoski, J., Brown, A. G. A., Vallenari, A., Prusti, T., de Bruijne, J. H. J., Bailer-Jones, C. A. L., Evans, D. W., Eyer, L., Jansen, F., Klioner, S. A., Lammers, U., Luri, X., Mignard, F., Panem, C., Pourbaix, D., Randich, S., Sartoretti, P., Siddiqui, H. I., Soubiran, C., Walton, N. A., Cropper, M., Drimmel, R., Katz, D., Lattanzi, M. G., Bakker, J., Cacciari, C., Castañeda, J., Chaoul, L., Cheek, N., Angeli, F. D., Fabricius, C., Guerra, R., Holl, B., Masana, E., Messineo, R., Mowlavi, N., Nienartowicz, K., Panuzzo, P., Portell, J., Riello, M., Seabroke, G. M., Tanga, P., Thévenin, F., Gracia-Abril, G., Comoretto, G., Garcia-Reinaldos, M., Teyssier, D., Altmann, M., Andrae, R., Audard, M., Bellas-Velidis, I., Benson, K., Berthier, J., Blomme, R., Burgess, P., Busso, G., Carry, B., Cellino, A., Clementini, G., Clotet, M., Creevey, O., Davidson, M., Ridder, J. D., Delchambre, L., Dell'Oro, A., Ducourant, C., Fernández-Hernández, J., Fouesneau, M., Frémat, Y., Galluccio, L., García–Torres, M., González-Núñez, J., González–Vidal, J. J., Gosset, E., Guy, L. P., Halbwachs, J.-L., Hambly, N. C., Harrison, D. L., Hernández, J., Hestroffer, D., Hodgkin, S. T., Hutton, A., Jasniewicz, G., Jean-Antoine-Piccolo, A., Jordan, S., Korn, A. J., Krone-Martins, A., Lanzafame, A. C., Lebzelter, T., Löffler, W., Manteiga, M., Marrese, P. M., Martín–Fleitas, J. M., Moitinho, A., Mora, A., Muinonen, K., Osinde, J., Pauwels, T., Petit, J.-M., Recio-Blanco, A., Richards, P. J., Rimoldini, L., Sarro, L. M., Siopis, C., Smith, M., Sozzetti, A., Süveges, M., Torra, J., van Reeven, W., Abbas, U., Aramburu, A. A., Accart, S., Aerts, C., Altavilla, G., Álvarez, M. A., Alvarez, R., Alves, J., Anderson, R. I., Andrei, A. H., Varela, E. A., Antiche, E., Arcay, B., Astraatmadja, T. L., Bach, N., Baker, S. G., Balaguer-Núñez, L., Balm, P., Barache, C., Barata, C., Barbato, D., Barblan, F., Barklem, P. S., Barrado, D., Barros, M., Barstow, M. A., Muñoz, S. B., Bassilana, J.-L., Becciani, U., Bellazzini, M., Berihuete, A., Bertone, S., Bianchi, L., Bienaymé, O., Blanco-Cuaresma, S., Boch, T., Boeche, C., Bombrun, A., Borrachero, R., Bossini, D., Bouquillon, S., Bourda, G., Bragaglia, A., Bramante, L., Bressan, A., Brouillet, N., Brüsemeister, T., Brugaletta, E., Bucciarelli, B., Burlacu, A., Busonero, D., Butkevich, A. G., Buzzi, R., Caffau, E., Cancelliere, R., Cannizzaro, G., Cantat-Gaudin, T., Carballo, R., Carlucci, T., Carrasco, J. M., Casamiquela, L., Castellani, M., Castro-Ginard, A., Charlot, P., Chemin, L., Chiavassa, A., Cocozza, G., Costigan, G., Cowell, S., Crifo, F., Crosta, M., Crowley, C., Cuypers, J., Dafonte, C., Damerdji, Y., Dapergolas, A., David, P., David, M., de Laverny, P., Luise, F. D., March, R. D., de Martino, D., de Souza, R., de Torres, A., Debosscher, J., del Pozo, E., Delbo, M., Delgado, A., Delgado, H. E., Matteo, P. D., Diakite, S., Diener, C., Distefano, E., Dolding, C., Drazinos, P., Durán, J., Edvardsson, B., Enke, H., Eriksson, K., Esquej, P., Bontemps, G. E., Fabre, C., Fabrizio,

M., Faigler, S., Falcão, A. J., Casas, M. F., Federici, L., Fedorets, G., Fernique, P., Figueras, F., Filippi, F., Findeisen, K., Fonti, A., Fraile, E., Fraser, M., Frézouls, B., Gai, M., Galleti, S., Garabato, D., García–Sedano, F., Garofalo, A., Garralda, N., Gavel, A., Gavras, P., Gerssen, J., Geyer, R., Giacobbe, P., Gilmore, G., Girona, S., Giuffrida, G., Glass, F., Gomes, M., Granvik, M., Gueguen, A., Guerrier, A., Guiraud, J., Gutiérrez–Sánchez, R., Haigron, R., Hatzidimitriou, D., Hauser, M., Haywood, M., Heiter, U., Heu, J., Hilger, T., Hofmann, W., Holland, G., Huckle, H. E., Hypki, A., Icardi, V., Janßen, K., de Fombelle, G. J., Jonker, P. G., Juhász, Á. L., Julbe, F., Karampelas, A., Kewley, A., Klar, J., Kochoska, A., Kohley, R., Kolenberg, K., Kontizas, M., Kontizas, E., Koposov, S. E., Kordopatis, G., Kostrzewa-Rutkowska, Z., Koubsky, P., Lambert, S., Lanza, A. F., Lasne, Y., Lavigne, J.-B., Fustec, Y. L., Poncin-Lafitte, C. L., Lebreton, Y., Leccia, S., Leclerc, N., Lecoeur-Taibi, I., Lenhardt, H., Leroux, F., Liao, S., Licata, E., Lindstrøm, H. E. P., Lister, T. A., Livanou, E., Lobel, A., López, M., Managau, S., Mann, R. G., Mantelet, G., Marchal, O., Marchant, J. M., Marconi, M., Marinoni, S., Marschalkó, G., Marshall, D. J., Martino, M., Marton, G., Mary, N., Matijevič, G., Mazeh, T., Messina, S., Michalik, D., Millar, N. R., Molina, D., Molinaro, R., Molnár, L., Montegriffo, P., Mor, R., Morbidelli, R., Morel, T., Morris, D., Mulone, A. F., Muraveva, T., Musella, I., Nelemans, G., Nicastro, L., Noval, L., O'Mullane, W., Ordénovic, C., Ordóñez–Blanco, D., Osborne, P., Pagani, C., Pagano, I., Pailler, F., Palacin, H., Palaversa, L., Panahi, A., Pawlak, M., Piersimoni, A. M., Pineau, F.-X., Plachy, E., Plum, G., Poggio, E., Poujoulet, E., Prša, A., Pulone, L., Racero, E., Ragaini, S., Rambaux, N., Ramos-Lerate, M., Regibo, S., Riclet, F., Ripepi, V., Riva, A., Rivard, A., Rixon, G., Roegiers, T., Roelens, M., Romero-Gómez, M., Rowell, N., Royer, F., Ruiz-Dern, L., Sadowski, G., Sellés, T. S., Sahlmann, J., Salgado, J., Salguero, E., Sanna, N., Santana-Ros, T., Sarasso, M., Savietto, H., Schultheis, M., Sciacca, E., Segol, M., Segovia, J. C., Ségransan, D., Shih, I.-C., Siltala, L., Silva, A. F., Smart, R. L., Smith, K. W., Solano, E., Solitro, F., Sordo, R., Nieto, S. S., Souchay, J., Spagna, A., Spoto, F., Stampa, U., Steele, I. A., Steidelmüller, H., Stephenson, C. A., Stoev, H., Suess, F. F., Surdej, J., Szabados, L., Szegedi-Elek, E., Tapiador, D., Taris, F., Tauran, G., Taylor, M. B., Teixeira, R., Terrett, D., Teyssandier, P., Thuillot, W., Titarenko, A., Clotet, F. T., Turon, C., Ulla, A., Utrilla, E., Uzzi, S., Vaillant, M., Valentini, G., Valette, V., van Elteren, A., Hemelryck, E. V., van Leeuwen, M., Vaschetto, M., Vecchiato, A., Viala, Y., Vicente, D., Vogt, S., von Essen, C., Voss, H., Votruba, V., Voutsinas, S., Walmsley, G., Weiler, M., Wertz, O., Wevems, T., Wyrzykowski, Ł., Yoldas, A., Žerjal, M., Ziaeepour, H., Zorec, J., Zschocke, S., Zucker, S., Zurbach, C., and Zwitter, T. (2018). igaia/idata release 2. *Astronomy &amp Astrophysics*, 616:A12.

Colpi, M., Mapelli, M., and Possenti, A. (2003). Probing the Presence of a Single or Binary Black Hole in the Globular Cluster NGC 6752 with Pulsar Dynamics. *The Astrophysical Journal*, 599(2):1260–1271.

Colpi, M., Possenti, A., and Gualandris, A. (2002). The Case of PSR J1911-5958A

in the Outskirts of NGC 6752: Signature of a Black Hole Binary in the Cluster Core? *Astrophysical Journal, Letters*, 570(2):L85–L88.

Dall'Amico, M., Mapelli, M., Carlo, U. N. D., Bouffanais, Y., Rastello, S., Santoliquido, F., Ballone, A., and Sedda, M. A. (2021). Gw190521 formation via three-body encounters in young massive star clusters.

Davenport, J. R. A. and Sandquist, E. L. (2010). Death of a Cluster: The Destruction of M67 as Seen by the Sloan Digital Sky Survey. *The Astrophysical Journal*, 711(2):559–572.

Fujii, M. S. and Portegies Zwart, S. (2014). The moment of core collapse in star clusters with a mass function. *Monthly Notices of the Royal Astronomical Society*, 439(1):1003–1014.

Gaia Collaboration, Babusiaux, C., van Leeuwen, F., Barstow, M. A., Jordi, C., Vallenari, A., Bossini, D., Bressan, A., Cantat-Gaudin, T., van Leeuwen, M., Brown, A. G. A., Prusti, T., de Bruijne, J. H. J., Bailer-Jones, C. A. L., Biermann, M., Evans, D. W., Eyer, L., Jansen, F., Klioner, S. A., Lammers, U., Lindegren, L., Luri, X., Mignard, F., Panem, C., Pourbaix, D., Randich, S., Sartoretti, P., Siddiqui, H. I., Soubiran, C., Walton, N. A., Arenou, F., Bastian, U., Cropper, M., Drimmel, R., Katz, D., Lattanzi, M. G., Bakker, J., Cacciari, C., Castañeda, J., Chaoul, L., Cheek, N., De Angeli, F., Fabricius, C., Guerra, R., Holl, B., Masana, E., Messineo, R., Mowlavi, N., Nienartowicz, K., Panuzzo, P., Portell, J., Riello, M., Seabroke, G. M., Tanga, P., Thévenin, F., Gracia-Abril, G., Comoretto, G., Garcia-Reinaldos, M., Teyssier, D., Altmann, M., Andrae, R., Audard, M., Bellas-Velidis, I., Benson, K., Berthier, J., Blomme, R., Burgess, P., Busso, G., Carry, B., Cellino, A., Clementini, G., Clotet, M., Creevey, O., Davidson, M., De Ridder, J., Delchambre, L., Dell´Oro, A., Ducourant, C., Fernández-Hernández, J., Fouesneau, M., Frémat, Y., Galluccio, L., García-Torres, M., González-Núñez, J., González-Vidal, J. J., Gosset, E., Guy, L. P., Halbwachs, J.-L., Hambly, N. C., Harrison, D. L., Hernández, J., Hestroffer, D., Hodgkin, S. T., Hutton, A., Jasniewicz, G., Jean-Antoine-Piccolo, A., Jordan, S., Korn, A. J., Krone-Martins, A., Lanzafame, A. C., Lebzelter, T., Löffler, W., Manteiga, M., Marrese, P. M., Martín-Fleitas, J. M., Moitinho, A., Mora, A., Muinonen, K., Osinde, J., Pancino, E., Pauwels, T., Petit, J.-M., Recio-Blanco, A., Richards, P. J., Rimoldini, L., Robin, A. C., Sarro, L. M., Siopis, C., Smith, M., Sozzetti, A., Süveges, M., Torra, J., van Reeven, W., Abbas, U., Abreu Aramburu, A., Accart, S., Aerts, C., Altavilla, G., Álvarez, M. A., Alvarez, R., Alves, J., Anderson, R. I., Andrei, A. H., Anglada Varela, E., Antiche, E., Antoja, T., Arcay, B., Astraatmadja, T. L., Bach, N., Baker, S. G., Balaguer-Núñez, L., Balm, P., Barache, C., Barata, C., Barbato, D., Barblan, F., Barklem, P. S., Barrado, D., Barros, M., Bartholomé Muñoz, L., Bassilana, J.-L., Becciani, U., Bellazzini, M., Berihuete, A., Bertone, S., Bianchi, L., Bienaymé, O., Blanco-Cuaresma, S., Boch, T., Boeche, C., Bombrun, A., Borrachero, R., Bouquillon, S., Bourda, G., Bragaglia, A., Bramante, L., Breddels, M. A., Brouillet, N., Brüsemeister, T., Brugaletta, E., Bucciarelli, B., Burlacu,

A., Busonero, D., Butkevich, A. G., Buzzi, R., Caffau, E., Cancelliere, R., Cannizzaro, G., Carballo, R., Carlucci, T., Carrasco, J. M., Casamiquela, L., Castellani, M., Castro-Ginard, A., Charlot, P., Chemin, L., Chiavassa, A., Cocozza, G., Costigan, G., Cowell, S., Crifo, F., Crosta, M., Crowley, C., Cuypers, J., Dafonte, C., Damerdji, Y., Dapergolas, A., David, P., David, M., de Laverny, P., De Luise, F., De March, R., de Martino, D., de Souza, R., de Torres, A., Debosscher, J., del Pozo, E., Delbo, M., Delgado, A., Delgado, H. E., Diakite, S., Diener, C., Distefano, E., Dolding, C., Drazinos, P., Durán, J., Edvardsson, B., Enke, H., Eriksson, K., Esquej, P., Eynard Bontemps, G., Fabre, C., Fabrizio, M., Faigler, S., Falcão, A. J., Farràs Casas, M., Federici, L., Fedorets, G., Fernique, P., Figueras, F., Filippi, F., Findeisen, K., Fonti, A., Fraile, E., Fraser, M., Frézouls, B., Gai, M., Galleti, S., Garabato, D., García-Sedano, F., Garofalo, A., Garralda, N., Gavel, A., Gavras, P., Gerssen, J., Geyer, R., Giacobbe, P., Gilmore, G., Girona, S., Giuffrida, G., Glass, F., Gomes, M., Granvik, M., Gueguen, A., Guerrier, A., Guiraud, J., Gutié, R., Haigron, R., Hatzidimitriou, D., Hauser, M., Haywood, M., Heiter, U., Helmi, A., Heu, J., Hilger, T., Hobbs, D., Hofmann, W., Holland, G., Huckle, H. E., Hypki, A., Icardi, V., Janßen, K., Jevardat de Fombelle, G., Jonker, P. G., Juhász, Á. L., Julbe, F., Karampelas, A., Kewley, A., Klar, J., Kochoska, A., Kohley, R., Kolenberg, K., Kontizas, M., Kontizas, E., Koposov, S. E., Kordopatis, G., Kostrzewa-Rutkowska, Z., Koubsky, P., Lambert, S., Lanza, A. F., Lasne, Y., Lavigne, J.-B., Le Fustec, Y., Le Poncin-Lafitte, C., Lebreton, Y., Leccia, S., Leclerc, N., Lecoeur-Taibi, I., Lenhardt, H., Leroux, F., Liao, S., Licata, E., Lindstrøm, H. E. P., Lister, T. A., Livanou, E., Lobel, A., López, M., Managau, S., Mann, R. G., Mantelet, G., Marchal, O., Marchant, J. M., Marconi, M., Marinoni, S., Marschalkó, G., Marshall, D. J., Martino, M., Marton, G., Mary, N., Massari, D., Matijevic, G., Mazeh, T., McMillan, P. J., Messina, S., Michalik, D., Millar, N. R., Molina, D., Molinaro, R., Molnár, L., Montegriffo, P., Mor, R., Morbidelli, R., Morel, T., Morris, D., Mulone, A. F., Muraveva, T., Musella, I., Nelemans, G., Nicastro, L., Noval, L., O´Mullane, W., Ordénovic, C., Ordóñez-Blanco, D., Osborne, P., Pagani, C., Pagano, I., Pailler, F., Palacin, H., Palaversa, L., Panahi, A., Pawlak, M., Piersimoni, A. M., Pineau, F.-X., Plachy, E., Plum, G., Poggio, E., Poujoulet, E., Prsa, A., Pulone, L., Racero, E., Ragaini, S., Rambaux, N., Ramos-Lerate, M., Regibo, S., Reylé, C., Riclet, F., Ripepi, V., Riva, A., Rivard, A., Rixon, G., Roegiers, T., Roelens, M., Romero-Gómez, M., Rowell, N., Royer, F., Ruiz-Dern, L., Sadowski, G., Sagristà Sellés, T., Sahlmann, J., Salgado, J., Salguero, E., Sanna, N., Santana-Ros, T., Sarasso, M., Savietto, H., Schultheis, M., Sciacca, E., Segol, M., Segovia, J. C., Ségransan, D., Shih, I-C., Siltala, L., Silva, A. F., Smart, R. L., Smith, K. W., Solano, E., Solitro, F., Sordo, R., Soria Nieto, S., Souchay, J., Spagna, A., Spoto, F., Stampa, U., Steele, I. A., Steidelmüller, H., Stephenson, C. A., Stoev, H., Suess, F. F., Surdej, J., Szabados, L., Szegedi-Elek, E., Tapiador, D., Taris, F., Tauran, G., Taylor, M. B., Teixeira, R., Terrett, D., Teyssandier, P., Thuillot, W., Titarenko, A., Torra Clotet, F., Turon, C., Ulla, A., Utrilla, E., Uzzi, S., Vaillant, M., Valentini, G., Valette, V., van Elteren,

A., Van Hemelryck, E., Vaschetto, M., Vecchiato, A., Veljanoski, J., Viala, Y., Vicente, D., Vogt, S., von Essen, C., Voss, H., Votruba, V., Voutsinas, S., Walmsley, G., Weiler, M., Wertz, O., Wevers, T., Wyrzykowski, L., Yoldas, A., Zerjal, M., Ziaeepour, H., Zorec, J., Zschocke, S., Zucker, S., Zurbach, C., and Zwitter, and T. (2018). Gaia data release 2 - observational hertzsprung-russell diagrams. *A&A*, 616:A10.

Gaia Collaboration, Brown, A. G. A., Vallenari, A., Prusti, T., de Bruijne, J. H. J., Babusiaux, C., Biermann, M., Creevey, O. L., Evans, D. W., Eyer, L., Hutton, A., Jansen, F., Jordi, C., Klioner, S. A., Lammers, U., Lindegren, L., Luri, X., Mignard, F., Panem, C., Pourbaix, D., Randich, S., Sartoretti, P., Soubiran, C., Walton, N. A., Arenou, F., Bailer-Jones, C. A. L., Bastian, U., Cropper, M., Drimmel, R., Katz, D., Lattanzi, M. G., van Leeuwen, F., Bakker, J., Cacciari, C., Castañeda, J., De Angeli, F., Ducourant, C., Fabricius, C., Fouesneau, M., Frémat, Y., Guerra, R., Guerrier, A., Guiraud, J., Jean-Antoine Piccolo, A., Masana, E., Messineo, R., Mowlavi, N., Nicolas, C., Nienartowicz, K., Pailler, F., Panuzzo, P., Riclet, F., Roux, W., Seabroke, G. M., Sordo, R., Tanga, P., Thévenin, F., Gracia-Abril, G., Portell, J., Teyssier, D., Altmann, M., Andrae, R., Bellas-Velidis, I., Benson, K., Berthier, J., Blomme, R., Brugaletta, E., Burgess, P. W., Busso, G., Carry, B., Cellino, A., Cheek, N., Clementini, G., Damerdji, Y., Davidson, M., Delchambre, L., Dell'Oro, A., Fernández-Hernández, J., Galluccio, L., García-Lario, P., Garcia-Reinaldos, M., González-Núñez, J., Gosset, E., Haigron, R., Halbwachs, J. L., Hambly, N. C., Harrison, D. L., Hatzidimitriou, D., Heiter, U., Hernández, J., Hestroffer, D., Hodgkin, S. T., Holl, B., Janßen, K., Jevardat de Fombelle, G., Jordan, S., Krone-Martins, A., Lanzafame, A. C., Löffler, W., Lorca, A., Manteiga, M., Marchal, O., Marrese, P. M., Moitinho, A., Mora, A., Muinonen, K., Osborne, P., Pancino, E., Pauwels, T., Petit, J. M., Recio-Blanco, A., Richards, P. J., Riello, M., Rimoldini, L., Robin, A. C., Roegiers, T., Rybizki, J., Sarro, L. M., Siopis, C., Smith, M., Sozzetti, A., Ulla, A., Utrilla, E., van Leeuwen, M., van Reeven, W., Abbas, U., Abreu Aramburu, A., Accart, S., Aerts, C., Aguado, J. J., Ajaj, M., Altavilla, G., Álvarez, M. A., Álvarez Cid-Fuentes, J., Alves, J., Anderson, R. I., Anglada Varela, E., Antoja, T., Audard, M., Baines, D., Baker, S. G., Balaguer-Núñez, L., Balbinot, E., Balog, Z., Barache, C., Barbato, D., Barros, M., Barstow, M. A., Bartolomé, S., Bassilana, J. L., Bauchet, N., Baudesson-Stella, A., Becciani, U., Bellazzini, M., Bernet, M., Bertone, S., Bianchi, L., Blanco-Cuaresma, S., Boch, T., Bombrun, A., Bossini, D., Bouquillon, S., Bragaglia, A., Bramante, L., Breedt, E., Bressan, A., Brouillet, N., Bucciarelli, B., Burlacu, A., Busonero, D., Butkevich, A. G., Buzzi, R., Caffau, E., Cancelliere, R., Cánovas, H., Cantat-Gaudin, T., Carballo, R., Carlucci, T., Carnerero, M. I., Carrasco, J. M., Casamiquela, L., Castellani, M., Castro-Ginard, A., Castro Sampol, P., Chaoul, L., Charlot, P., Chemin, L., Chiavassa, A., Cioni, M. R. L., Comoretto, G., Cooper, W. J., Cornez, T., Cowell, S., Crifo, F., Crosta, M., Crowley, C., Dafonte, C., Dapergolas, A., David, M., David, P., de Laverny, P., De Luise, F., De March, R., De Ridder, J., de Souza, R., de Teodoro, P., de Torres, A., del Peloso, E. F., del Pozo, E.,

Delbo, M., Delgado, A., Delgado, H. E., Delisle, J. B., Di Matteo, P., Diakite, S., Diener, C., Distefano, E., Dolding, C., Eappachen, D., Edvardsson, B., Enke, H., Esquej, P., Fabre, C., Fabrizio, M., Faigler, S., Fedorets, G., Fernique, P., Fienga, A., Figueras, F., Fouron, C., Fragkoudi, F., Fraile, E., Franke, F., Gai, M., Garabato, D., Garcia-Gutierrez, A., García-Torres, M., Garofalo, A., Gavras, P., Gerlach, E., Geyer, R., Giacobbe, P., Gilmore, G., Girona, S., Giuffrida, G., Gomel, R., Gomez, A., Gonzalez-Santamaria, I., González-Vidal, J. J., Granvik, M., Gutiérrez-Sánchez, R., Guy, L. P., Hauser, M., Haywood, M., Helmi, A., Hidalgo, S. L., Hilger, T., Hładczuk, N., Hobbs, D., Holland, G., Huckle, H. E., Jasniewicz, G., Jonker, P. G., Juaristi Campillo, J., Julbe, F., Karbevska, L., Kervella, P., Khanna, S., Kochoska, A., Kontizas, M., Kordopatis, G., Korn, A. J., Kostrzewa-Rutkowska, Z., Kruszyńska, K., Lambert, S., Lanza, A. F., Lasne, Y., Le Campion, J. F., Le Fustec, Y., Lebreton, Y., Lebzelter, T., Leccia, S., Leclerc, N., Lecoeur-Taibi, I., Liao, S., Licata, E., Lindstrøm, E. P., Lister, T. A., Livanou, E., Lobel, A., Madrero Pardo, P., Managau, S., Mann, R. G., Marchant, J. M., Marconi, M., Marcos Santos, M. M. S., Marinoni, S., Marocco, F., Marshall, D. J., Martin Polo, L., Martín-Fleitas, J. M., Masip, A., Massari, D., Mastrobuono-Battisti, A., Mazeh, T., McMillan, P. J., Messina, S., Michalik, D., Millar, N. R., Mints, A., Molina, D., Molinaro, R., Molnár, L., Montegriffo, P., Mor, R., Morbidelli, R., Morel, T., Morris, D., Mulone, A. F., Munoz, D., Muraveva, T., Murphy, C. P., Musella, I., Noval, L., Ordénovic, C., Orrù, G., Osinde, J., Pagani, C., Pagano, I., Palaversa, L., Palicio, P. A., Panahi, A., Pawlak, M., Peñalosa Esteller, X., Penttilä, A., Piersimoni, A. M., Pineau, F. X., Plachy, E., Plum, G., Poggio, E., Poretti, E., Poujoulet, E., Prša, A., Pulone, L., Racero, E., Ragaini, S., Rainer, M., Raiteri, C. M., Rambaux, N., Ramos, P., Ramos-Lerate, M., Re Fiorentin, P., Regibo, S., Reylé, C., Ripepi, V., Riva, A., Rixon, G., Robichon, N., Robin, C., Roelens, M., Rohrbasser, L., Romero-Gómez, M., Rowell, N., Royer, F., Rybicki, K. A., Sadowski, G., Sagristà Sellés, A., Sahlmann, J., Salgado, J., Salguero, E., Samaras, N., Sanchez Gimenez, V., Sanna, N., Santoveña, R., Sarasso, M., Schultheis, M., Sciacca, E., Segol, M., Segovia, J. C., Ségransan, D., Semeux, D., Shahaf, S., Siddiqui, H. I., Siebert, A., Siltala, L., Slezak, E., Smart, R. L., Solano, E., Solitro, F., Souami, D., Souchay, J., Spagna, A., Spoto, F., Steele, I. A., Steidelmüller, H., Stephenson, C. A., Süveges, M., Szabados, L., Szegedi-Elek, E., Taris, F., Tauran, G., Taylor, M. B., Teixeira, R., Thuillot, W., Tonello, N., Torra, F., Torra, J., Turon, C., Unger, N., Vaillant, M., van Dillen, E., Vanel, O., Vecchiato, A., Viala, Y., Vicente, D., Voutsinas, S., Weiler, M., Wevers, T., Wyrzykowski, Ł., Yoldas, A., Yvard, P., Zhao, H., Zorec, J., Zucker, S., Zurbach, C., and Zwitter, T. (2021). Gaia Early Data Release 3. Summary of the contents and survey properties. *Astronomy and Astrophysics*, 649:A1.

Gaia Collaboration, Vallenari, A., Brown, A. G. A., Prusti, T., de Bruijne, J. H. J., Arenou, F., Babusiaux, C., Biermann, M., Creevey, O. L., Ducourant, C., Evans, D. W., Eyer, L., Guerra, R., Hutton, A., Jordi, C., Klioner, S. A., Lammers, U. L., Lindegren, L., Luri, X., Mignard, F., Panem, C., Pourbaix, D., Randich, S., Sartoretti, P., Soubiran, C., Tanga, P., Walton, N. A., Bailer-Jones, C. A. L.,

Bastian, U., Drimmel, R., Jansen, F., Katz, D., Lattanzi, M. G., van Leeuwen, F., Bakker, J., Cacciari, C., Castañeda, J., De Angeli, F., Fabricius, C., Fouesneau, M., Frémat, Y., Galluccio, L., Guerrier, A., Heiter, U., Masana, E., Messineo, R., Mowlavi, N., Nicolas, C., Nienartowicz, K., Pailler, F., Panuzzo, P., Riclet, F., Roux, W., Seabroke, G. M., Sordoørcit, R., Thévenin, F., Gracia-Abril, G., Portell, J., Teyssier, D., Altmann, M., Andrae, R., Audard, M., Bellas-Velidis, I., Benson, K., Berthier, J., Blomme, R., Burgess, P. W., Busonero, D., Busso, G., Cánovas, H., Carry, B., Cellino, A., Cheek, N., Clementini, G., Damerdji, Y., Davidson, M., de Teodoro, P., Nuñez Campos, M., Delchambre, L., Dell'Oro, A., Esquej, P., Fernández-Hernández, J., Fraile, E., Garabato, D., García-Lario, P., Gosset, E., Haigron, R., Halbwachs, J. L., Hambly, N. C., Harrison, D. L., Hernández, J., Hestroffer, D., Hodgkin, S. T., Holl, B., Janßen, K., Jevardat de Fombelle, G., Jordan, S., Krone-Martins, A., Lanzafame, A. C., Löffler, W., Marchal, O., Marrese, P. M., Moitinho, A., Muinonen, K., Osborne, P., Pancino, E., Pauwels, T., Recio-Blanco, A., Reylé, C., Riello, M., Rimoldini, L., Roegiers, T., Rybizki, J., Sarro, L. M., Siopis, C., Smith, M., Sozzetti, A., Utrilla, E., van Leeuwen, M., Abbas, U., Ábrahám, P., Abreu Aramburu, A., Aerts, C., Aguado, J. J., Ajaj, M., Aldea-Montero, F., Altavilla, G., Álvarez, M. A., Alves, J., Anders, F., Anderson, R. I., Anglada Varela, E., Antoja, T., Baines, D., Baker, S. G., Balaguer-Núñez, L., Balbinot, E., Balog, Z., Barache, C., Barbato, D., Barros, M., Barstow, M. A., Bartolomé, S., Bassilana, J. L., Bauchet, N., Becciani, U., Bellazzini, M., Berihuete, A., Bernet, M., Bertone, S., Bianchi, L., Binnenfeld, A., Blanco-Cuaresma, S., Blazere, A., Boch, T., Bombrun, A., Bossini, D., Bouquillon, S., Bragaglia, A., Bramante, L., Breedt, E., Bressan, A., Brouillet, N., Brugaletta, E., Bucciarelli, B., Burlacu, A., Butkevich, A. G., Buzzi, R., Caffau, E., Cancelliere, R., Cantat-Gaudin, T., Carballo, R., Carlucci, T., Carnerero, M. I., Carrasco, J. M., Casamiquela, L., Castellani, M., Castro-Ginard, A., Chaoul, L., Charlot, P., Chemin, L., Chiaramida, V., Chiavassa, A., Chornay, N., Comoretto, G., Contursi, G., Cooper, W. J., Cornez, T., Cowell, S., Crifo, F., Cropper, M., Crosta, M., Crowley, C., Dafonte, C., Dapergolas, A., David, M., David, P., de Laverny, P., De Luise, F., De March, R., De Ridder, J., de Souza, R., de Torres, A., del Peloso, E. F., del Pozo, E., Delbo, M., Delgado, A., Delisle, J. B., Demouchy, C., Dharmawardena, T. E., Di Matteo, P., Diakite, S., Diener, C., Distefano, E., Dolding, C., Edvardsson, B., Enke, H., Fabre, C., Fabrizio, M., Faigler, S., Fedorets, G., Fernique, P., Fienga, A., Figueras, F., Fournier, Y., Fouron, C., Fragkoudi, F., Gai, M., Garcia-Gutierrez, A., Garcia-Reinaldos, M., García-Torres, M., Garofalo, A., Gavel, A., Gavras, P., Gerlach, E., Geyer, R., Giacobbe, P., Gilmore, G., Girona, S., Giuffrida, G., Gomel, R., Gomez, A., González-Núñez, J., González-Santamaría, I., González-Vidal, J. J., Granvik, M., Guillout, P., Guiraud, J., Gutiérrez-Sánchez, R., Guy, L. P., Hatzidimitriou, D., Hauser, M., Haywood, M., Helmer, A., Helmi, A., Sarmiento, M. H., Hidalgo, S. L., Hilger, T., Hładczuk, N., Hobbs, D., Holland, G., Huckle, H. E., Jardine, K., Jasniewicz, G., Jean-Antoine Piccolo, A., Jiménez-Arranz, Ó., Jorissen, A., Juaristi Campillo, J., Julbe, F., Karbevska, L., Kervella, P., Khanna, S., Kontizas, M., Kordopatis, G., Korn, A. J., Kóspál,

Á., Kostrzewa-Rutkowska, Z., Kruszyńska, K., Kun, M., Laizeau, P., Lambert, S., Lanza, A. F., Lasne, Y., Le Campion, J. F., Lebreton, Y., Lebzelter, T., Leccia, S., Leclerc, N., Lecoeur-Taibi, I., Liao, S., Licata, E. L., Lindstrøm, H. E. P., Lister, T. A., Livanou, E., Lobel, A., Lorca, A., Loup, C., Madrero Pardo, P., Magdaleno Romeo, A., Managau, S., Mann, R. G., Manteiga, M., Marchant, J. M., Marconi, M., Marcos, J., Marcos Santos, M. M. S., Marín Pina, D., Marinoni, S., Marocco, F., Marshall, D. J., Polo, L. M., Martín-Fleitas, J. M., Marton, G., Mary, N., Masip, A., Massari, D., Mastrobuono-Battisti, A., Mazeh, T., McMillan, P. J., Messina, S., Michalik, D., Millar, N. R., Mints, A., Molina, D., Molinaro, R., Molnár, L., Monari, G., Monguió, M., Montegriffo, P., Montero, A., Mor, R., Mora, A., Morbidelli, R., Morel, T., Morris, D., Muraveva, T., Murphy, C. P., Musella, I., Nagy, Z., Noval, L., Ocaña, F., Ogden, A., Ordenovic, C., Osinde, J. O., Pagani, C., Pagano, I., Palaversa, L., Palicio, P. A., Pallas-Quintela, L., Panahi, A., Payne-Wardenaar, S., Peñalosa Esteller, X., Penttilä, A., Pichon, B., Piersimoni, A. M., Pineau, F. X., Plachy, E., Plum, G., Poggio, E., Prša, A., Pulone, L., Racero, E., Ragaini, S., Rainer, M., Raiteri, C. M., Rambaux, N., Ramos, P., Ramos-Lerate, M., Re Fiorentin, P., Regibo, S., Richards, P. J., Rios Diaz, C., Ripepi, V., Riva, A., Rix, H. W., Rixon, G., Robichon, N., Robin, A. C., Robin, C., Roelens, M., Rogues, H. R. O., Rohrbasser, L., Romero-Gómez, M., Rowell, N., Royer, F., Ruz Mieres, D., Rybicki, K. A., Sadowski, G., Sáez Núñez, A., Sagristà Sellés, A., Sahlmann, J., Salguero, E., Samaras, N., Sanchez Gimenez, V., Sanna, N., Santoveña, R., Sarasso, M., Schultheis, M., Sciacca, E., Segol, M., Segovia, J. C., Ségransan, D., Semeux, D., Shahaf, S., Siddiqui, H. I., Siebert, A., Siltala, L., Silvelo, A., Slezak, E., Slezak, I., Smart, R. L., Snaith, O. N., Solano, E., Solitro, F., Souami, D., Souchay, J., Spagna, A., Spina, L., Spoto, F., Steele, I. A., Steidelmüller, H., Stephenson, C. A., Süveges, M., Surdej, J., Szabados, L., Szegedi-Elek, E., Taris, F., Taylo, M. B., Teixeira, R., Tolomei, L., Tonello, N., Torra, F., Torra, J., Torralba Elipe, G., Trabucchi, M., Tsounis, A. T., Turon, C., Ulla, A., Unger, N., Vaillant, M. V., van Dillen, E., van Reeven, W., Vanel, O., Vecchiato, A., Viala, Y., Vicente, D., Voutsinas, S., Weiler, M., Wevers, T., Wyrzykowski, L., Yoldas, A., Yvard, P., Zhao, H., Zorec, J., Zucker, S., and Zwitter, T. (2022). Gaia Data Release 3: Summary of the content and survey properties. *arXiv e-prints*, page arXiv:2208.00211.

Geller, A. M., Latham, D. W., and Mathieu, R. D. (2015). STELLAR RADIAL VELOCITIES IN THE OLD OPEN CLUSTER m67 (NGC 2682). i. MEMBERSHIPS, BINARIES, AND KINEMATICS. *The Astronomical Journal*, 150(3):97.

Georgiev, I. Y., Hilker, M., Puzia, T. H., Goudfrooij, P., and Baumgardt, H. (2009). Globular cluster systems in nearby dwarf galaxies - II. Nuclear star clusters and their relation to massive Galactic globular clusters. *Monthly Notices of the Royal Astronomical Society*, 396(2):1075–1085.

Getman, K. V., Feigelson, E. D., Kuhn, M. A., and Garmire, G. P. (2019). Gaia stellar kinematics in the head of the Orion A cloud: runaway stellar groups

and gravitational infall. *Monthly Notices of the Royal Astronomical Society*, 487(3):2977–3000.

Grondin, S. M., Webb, J. J., Lane, J. M. M., Speagle, J. S., and Leigh, N. W. C. (2023a). A catalogue of Galactic GEMS: Globular cluster Extra-tidal Mock Stars. *arXiv e-prints*, page arXiv:2310.09331.

Grondin, S. M., Webb, J. J., Leigh, N. W. C., Speagle, J. S., and Khalifeh, R. J. (2023b). Searching for the extra-tidal stars of globular clusters using high-dimensional analysis and a core particle spray code. *Monthly Notices of the Royal Astronomical Society*, 518(3):4249–4264.

Grondin, S. M., Webb, J. J., Leigh, N. W. C., Speagle(), J. S., and Khalifeh, R. J. (2022). Searching for the extra-tidal stars of globular clusters using high-dimensional analysis and a core particle spray code. *Monthly Notices of the Royal Astronomical Society*, 518(3):4249–4264.

Gualandris, A., Portegies Zwart, S., and Eggleton, P. P. (2004). N-body simulations of stars escaping from the Orion nebula. *Monthly Notices of the Royal Astronomical Society*, 350(2):615–626.

Gvaramadze, V. V. and Gualandris, A. (2010). Very massive runaway stars from three-body encounters. *Monthly Notices of the Royal Astronomical Society*, 410(1):304–312.

Hamers, A. S. (2021). Multiple Stellar Evolution: a population synthesis algorithm to model the stellar, binary, and dynamical evolution of multiple-star systems. In Siebert, A., Baillié, K., Lagadec, E., Lagarde, N., Malzac, J., Marquette, J. B., N'Diaye, M., Richard, J., and Venot, O., editors, *SF2A-2021: Proceedings of the Annual meeting of the French Society of Astronomy and Astrophysics. Eds.: A. Siebert*, pages 457–462.

Hurley, J. R., Pols, O. R., Aarseth, S. J., and Tout, C. A. (2005). A complete N-body model of the old open cluster M67. *Monthly Notices of the Royal Astronomical Society*, 363(1):293–314.

Igoshev, A. P., Perets, H., and Hallakoun, N. (2022). Hyper-runaway and hypervelocity white dwarf candidates in Gaia Data Release 3: Possible remnants from Ia/Iax supernova explosions or dynamical encounters. *Monthly Notices of the Royal Astronomical Society*, 518(4):6223–6237.

Jacobson, H. R., Pilachowski, C. A., and Friel, E. D. (2011). A Chemical Abundance Study of 10 Open Clusters Based on WIYN-Hydra Spectroscopy. *Astronomical Journal*, 142(2):59.

Keenan, D. W., Innanen, K. A., and House, F. C. (1973). Galactic orbits and tidal radii of the Clusters M67, NGC 188 and W Centauri. *Astronomical Journal*, 78:173.

Kharchenko, N. V., Piskunov, A. E., Schilbach, E., Röser, S., and Scholz, R. D.

(2013). Global survey of star clusters in the Milky Way. II. The catalogue of basic parameters. *Astronomy and Astrophysics*, 558:A53.

Kuhn, M. A., Hillenbrand, L. A., Sills, A., Feigelson, E. D., and Getman, K. V. (2019). Kinematics in Young Star Clusters and Associations with Gaia DR2. *The Astrophysical Journal*, 870(1):32.

Leigh, N. and Geller, A. M. (2012). Small-N collisional dynamics: pushing into the realm of not-so-small N. *Monthly Notices of the Royal Astronomical Society*, 425(3):2369–2377.

Leigh, N. and Sills, A. (2011). An analytic technique for constraining the dynamical origins of multiple star systems containing merger products. *Monthly Notices of the Royal Astronomical Society*, 410(4):2370–2384.

Leigh, N. W. C. and Geller, A. M. (2013). The dynamical significance of triple star systems in star clusters. *Monthly Notices of the Royal Astronomical Society*, 432(3):2474–2479.

Leigh, N. W. C., Stone, N. C., Geller, A. M., Shara, M. M., Muddu, H., Solano-Oropeza, D., and Thomas, Y. (2016a). The chaotic four-body problem in Newtonian gravity- I. Identical point-particles. *Monthly Notices of the Royal Astronomical Society*, 463(3):3311–3325.

Leigh, N. W. C., Stone, N. C., Geller, A. M., Shara, M. M., Muddu, H., Solano-Oropeza, D., and Thomas, Y. (2016b). The chaotic four-body problem in Newtonian gravity- I. Identical point-particles. *Monthly Notices of the Royal Astronomical Society*, 463(3):3311–3325.

Leigh, N. W. C., Toonen, S., Portegies Zwart, S. F., and Perna, R. (2020). Mergers of equal-mass binaries with compact object companions from mass transfer in triple star systems. *Monthly Notices of the Royal Astronomical Society*, 496(2):1819–1833.

Leigh, N. W. C. and Wegsman, S. (2018). Illustrating chaos: a schematic discretization of the general three-body problem in newtonian gravity. *Monthly Notices of the Royal Astronomical Society*, 476(1):336–343.

Leonard, P. J. T. (1996). The Implications of the Binary Properties of the M67 Blue Stragglers. *The Astrophysical Journal*, 470:521.

Li, Q.-Z., Huang, Y., Dong, X.-B., Zhang, H.-W., Beers, T. C., and Yuan, Z. (2023). On the Origins of Extreme Velocity Stars as Revealed by Large-scale Galactic Surveys. *Astronomical Journal*, 166(1):12.

Liao, J., Du, C., Li, H., Ma, J., and Shi, J. (2023). Hypervelocity Stars Track Back to the Galactic Center in Gaia DR3. *Astrophysical Journal, Letters*, 944(2):L39.

Luri, X., Brown, A. G. A., Sarro, L. M., Arenou, F., Bailer-Jones, C. A. L., Castro-Ginard, A., de Bruijne, J., Prusti, T., Babusiaux, C., and Delgado,

H. E. (2018). Gaia Data Release 2. Using Gaia parallaxes. *Astronomy and Astrophysics*, 616:A9.

Nauenberg, M. (1972). Analytic Approximations to the Mass-Radius Relation and Energy of Zero-Temperature Stars. *The Astrophysical Journal*, 175:417.

Nelemans, G., Yungelson, L. R., Portegies Zwart, S. F., and Verbunt, F. (2001). Population synthesis for double white dwarfs . I. Close detached systems. *Astronomy and Astrophysics*, 365:491–507.

Ness, M., Rix, H.-W., Hogg, D. W., Casey, A. R., Holtzman, J., Fouesneau, M., Zasowski, G., Geisler, D., Shetrone, M., Minniti, D., Frinchaboy, P. M., and Roman-Lopes, A. (2018). Galactic doppelgängers: The chemical similarity among field stars and among stars with a common birth origin. *The Astrophysical Journal*, 853(2):198.

Oh, S., Kroupa, P., and Pflamm-Altenburg, J. (2015). DEPENDENCY OF DYNAMICAL EJECTIONS OF o STARS ON THE MASSES OF VERY YOUNG STAR CLUSTERS. *The Astrophysical Journal*, 805(2):92.

Pasquini, L., Melo, C., Chavero, C., Dravins, D., Ludwig, H. G., Bonifacio, P., and de La Reza, R. (2011). Gravitational redshifts in main-sequence and giant stars. *Astronomy and Astrophysics*, 526:A127.

Pelupessy, F. I., van Elteren, A., de Vries, N., McMillan, S. L. W., Drost, N., and Portegies Zwart, S. F. (2013). The Astrophysical Multipurpose Software Environment. *Astronomy and Astrophysics*, 557:A84.

Perets, H. B. and Šubr, L. (2012). The Properties of Dynamically Ejected Runaway and Hyper-runaway Stars. *The Astrophysical Journal*, 751(2):133.

Pflamm-Altenburg, J. and Kroupa, P. (2006). A highly abnormal massive star mass function in the Orion Nebula cluster and the dynamical decay of trapezium systems. *Monthly Notices of the Royal Astronomical Society*, 373(1):295–304.

Portegies Zwart, S. F. and Verbunt, F. (1996). Population synthesis of high-mass binaries. *Astronomy and Astrophysics*, 309:179–196.

Portegies Zwart, S. F. and Verbunt, F. (2012). SeBa: Stellar and binary evolution. Astrophysics Source Code Library, record ascl:1201.003.

Price-Jones, N., Bovy, J., Webb, J. J., Allende Prieto, C., Beaton, R., Brownstein, J. R., Cohen, R. E., Cunha, K., Donor, J., Frinchaboy, P. M., García-Hernández, D. A., Lane, R. R., Majewski, S. R., Nidever, D. L., and Roman-Lopes, A. (2020). Strong chemical tagging with APOGEE: 21 candidate star clusters that have dissolved across the Milky Way disc. *Monthly Notices of the Royal Astronomical Society*, 496(4):5101–5115.

Reipurth, B., Mikkola, S., Connelley, M., and Valtonen, M. (2010). Orphaned Protostars. *Astrophysical Journal, Letters*, 725(1):L56–L61.

Renzo, M., Zapartas, E., de Mink, S. E., Götberg, Y., Justham, S., Farmer, R. J., Izzard, R. G., Toonen, S., and Sana, H. (2019). Massive runaway and walkaway stars. *Astronomy Astrophysics*, 624:A66.

Ryu, T., Leigh, N. W. C., and Perna, R. (2017a). An analytic method for identifying dynamically formed runaway stars. *Monthly Notices of the Royal Astronomical Society*, 470(1):2–19.

Ryu, T., Leigh, N. W. C., and Perna, R. (2017b). An analytic method for identifying dynamically formed runaway stars. *Monthly Notices of the Royal Astronomical Society*, 470(1):2–19.

Ryu, T., Leigh, N. W. C., and Perna, R. (2017c). Formation of runaway stars in a star-cluster potential. *Monthly Notices of the Royal Astronomical Society*, 470(3):3049–3067.

Ryu, T., Leigh, N. W. C., and Perna, R. (2017d). Numerical study of N = 4 binary-binary scatterings in a background potential. *Monthly Notices of the Royal Astronomical Society*, 467(4):4447–4461.

Salomon, J. B., Ibata, R., Reylé, C., Famaey, B., Libeskind, N. I., McConnachie, A. W., and Hoffman, Y. (2020). The proper motion of andromeda from gaia edr3: confirming a nearly radial orbit.

Schoettler, C., de Bruijne, J., Vaher, E., and Parker, R. J. (2020). Runaway and walkaway stars from the ONC with Gaia DR2. *Monthly Notices of the Royal Astronomical Society*, 495(3):3104–3123.

Steinmetz, M., Matijevič, G., Enke, H., Zwitter, T., Guiglion, G., McMillan, P. J., Kordopatis, G., Valentini, M., Chiappini, C., Casagrande, L., Wojno, J., Anguiano, B., Bienaymé, O., Bijaoui, A., Binney, J., Burton, D., Cass, P., de Laverny, P., Fiegert, K., Freeman, K., Fulbright, J. P., Gibson, B. K., Gilmore, G., Grebel, E. K., Helmi, A., Kunder, A., Munari, U., Navarro, J. F., Parker, Q., Ruchti, G. R., Recio-Blanco, A., Reid, W., Seabroke, G. M., Siviero, A., Siebert, A., Stupar, M., Watson, F., Williams, M. E. K., Wyse, R. F. G., Anders, F., Antoja, T., Birko, D., Bland-Hawthorn, J., Bossini, D., García, R. A., Carrillo, I., Chaplin, W. J., Elsworth, Y., Famaey, B., Gerhard, O., Jofre, P., Just, A., Mathur, S., Miglio, A., Minchev, I., Monari, G., Mosser, B., Ritter, A., Rodrigues, T. S., Scholz, R.-D., Sharma, S., Sysoliatina, K., and RAVE Collaboration (2020). The Sixth Data Release of the Radial Velocity Experiment (RAVE). I. Survey Description, Spectra, and Radial Velocities. *Astronomical Journal*, 160(2):82.

Tauris, T. M. (2014). Maximum speed of hypervelocity stars ejected from binaries. *Monthly Notices of the Royal Astronomical Society: Letters*, 448(1):L6–L10.

Toonen, S. (2021). The evolution of stellar triples. In *AAS/Division of Dynamical Astronomy Meeting*, volume 53 of *AAS/Division of Dynamical Astronomy Meeting*, page 204.07.

Toonen, S., Nelemans, G., and Portegies Zwart, S. (2012). Supernova Type Ia progenitors from merging double white dwarfs. Using a new population synthesis model. *Astronomy and Astrophysics*, 546:A70.

Toonen, S., Perets, H. B., and Hamers, A. S. (2018). Rate of WD-WD head-on collisions in isolated triples is too low to explain standard type Ia supernovae. *Astronomy and Astrophysics*, 610:A22.

Valtonen, M. and Karttunen, H. (2006). *The Three-Body Problem*. Cambridge University Press.

van Leeuwen, F. (2009). Parallaxes and proper motions for 20 open clusters as based on the new hipparcos catalogue. *Astronomy &amp Astrophysics*, 497(1):209–242.

VandenBerg, D. A. and Stetson, P. B. (2004). On the Old Open Clusters M67 and NGC 188: Convective Core Overshooting, Color-Temperature Relations, Distances, and Ages. *Publications of the ASP*, 116(825):997–1011.

Viani, L. and Basu, S. (2017). Isochrones of m67 with an expanded set of parameters. *EPJ Web of Conferences*, 160:05005.

Weatherford, N. C., Kıroğlu, F., Fragione, G., Chatterjee, S., Kremer, K., and Rasio, F. A. (2023). Stellar Escape from Globular Clusters. I. Escape Mechanisms and Properties at Ejection. *The Astrophysical Journal*, 946(2):104.

Yadav, R. K. S., Bedin, L. R., Piotto, G., Anderson, J., Cassisi, S., Villanova, S., Platais, I., Pasquini, L., Momany, Y., and Sagar, R. (2008). Ground-based CCD astrometry with wide-field imagers. II. A star catalog for M 67: WFI@2.2 m MPG/ESO astrometry, FLAMES@VLT radial velocities. *Astronomy and Astrophysics*, 484(2):609–620.

Appendix A

Test

A1 Reference frame

In this section, we describe our chosen frame of reference and how we convert the available positions and proper motions into this reference system.

A1.1 Positions

We begin with the positions for all the sources in the catalog, which we first consider in a two dimensional frame. Using $\mu_{\alpha*} \equiv \mu_\alpha \cos\delta$, the coordinate transformations for the positions frame are:

$$\begin{aligned} x &= \cos\delta \sin(\alpha - \alpha_0) \\ y &= \sin\delta \cos\delta_0 - \cos\delta \sin\delta_0 \cos(\alpha - \alpha_0) \end{aligned} \tag{A1.1}$$

The positions of the sources are denoted by α (RA) and δ (Dec). The centre of the cluster is identified by its RA and Dec, taking values $\alpha_0 = 8^h51^m23^s.3$, $\delta_0 = +11°49'02"$ (J2000) (Jacobson et al., 2011)

A1.2 Proper motions

Our goal is to determine two components of stellar velocities based on the proper motions μ_α and μ_δ.

The apparent motions of stars within stellar systems can be influenced by perspective effects and the motion of the system's centre-of-mass, as noted in van Leeuwen (2009). In particular, the motion of a cluster in the radial direction can produce an effect known as "perspective expansion," which has been observed in Gaia measurements of globular clusters, many of which have radial velocities (RVs) reaching hundreds of kilometers per second Gaia Collaboration et al. (2018). A first-order approximation of perspective expansion can be derived from Equation 13 in van Leeuwen (2009). The equations for the additional shift in proper motion of a star are:

$$\begin{aligned} \Delta\mu_{\alpha*,\mathrm{per}} &\approx \Delta\alpha_{\mathrm{i}} \left(\mu_{\delta,0} \sin\delta_0 - \frac{v_{\mathrm{r}}\varpi_0}{\kappa} \cos\delta_0 \right), \\ \Delta\mu_{\delta,\mathrm{per}} &\approx -\Delta\alpha_i \mu_{\alpha*,0} \sin\delta_0 - \Delta\delta_{\mathrm{i}} \frac{v_{\mathrm{r}}\varpi_0}{\kappa}, \end{aligned} \tag{A1.2}$$

Here $\Delta\alpha_i$ and $\Delta\delta_i$ are the difference in right ascension and declination between the system centre-of-mass and an individual star. The proper motions in RA and Dec are, respectively, $\mu_{\delta,0} = -10.97$ mas yr^{-1} and $\mu_{\delta,0} = -2.9396$ mas/yr^{-1}. We assume $v_{\mathrm{r}} = 33.64 \pm 0.03$ km s^{-1} (Geller et al., 2015) for the radial velocity of the centre-of-mass motion of M67 and $\varpi_0 = 860$ pc for the cluster's parallax (Cantat-Gaudin et al., 2018). The conversion factor that converts mas yr^{-1} to km s^{-1} at a distance of 1 kpc is $\kappa = 4.74$. The first term in each equation accounts for motion within a spherical coordinate system, while the second term accounts for the perceived expansion or contraction of an object as its distance increases or decreases.

These contributions can be subtracted from the observed proper motions (relative to the system centre-of-mass) to isolate the influence of internal kinematics (Brown et al., 1997). We calculate the components of the corrected velocities parallel to lines of constant right ascension and declination:

$$\begin{aligned} \mu_{\alpha,\mathrm{rest}} &\approx -\kappa \left(\frac{\Delta\mu_{\alpha*,\mathrm{obs}} - \Delta\mu_{\alpha*,\mathrm{per}}}{\varpi_0} \right), \\ \mu_{\delta,\mathrm{rest}} &\approx \kappa \left(\frac{\Delta\mu_{\delta*,\mathrm{obs}} - \Delta\mu_{\delta*,\mathrm{per}}}{\varpi_0} \right) \end{aligned} \tag{A1.3}$$

with $\Delta\mu_{\alpha*,\mathrm{obs}} = \mu_{\alpha*} - \mu_{\alpha*,0}$ and $\Delta\mu_{\delta*,\mathrm{obs}} = \mu_{\delta} - \mu_{\delta,0}$ are the differences in proper motion in right ascension and declination, respectively, between an individual star and the system centre-of-mass. We have as a result the $\mu_{\alpha,\mathrm{rest}}$ and $\mu_{\delta,\mathrm{rest}}$ as the proper motions in the rest of frame calculated for RA and DEC. We then transform the velocities to a 2-D Cartesian coordinate system, v_x and v_y, using the orthographic projection (Colaboration et al., 2018):

$$\begin{aligned} v_{\mathrm{x}} &= \mu_{\alpha,\mathrm{rest}} \cos(\alpha - \alpha_0) - \mu_{\delta,\mathrm{rest}} \sin\delta \sin(\alpha - \alpha_0) \\ v_{\mathrm{y}} &= \mu_{\alpha,\mathrm{rest}} \sin\delta_0 \sin(\alpha - \alpha_0) + \\ &\quad \mu_{\delta,\mathrm{rest}} \left(\cos\delta \cos\delta_0 + \sin\delta \sin\delta_0 \cos(\alpha - \alpha_0)\right). \end{aligned} \tag{A1.4}$$

A1.3 Cross Point of the stars

We use the following equation to find the cross-point:

$$\vec{X} = \lambda\hat{n} + \vec{X}_0, \tag{A1.5}$$

with $\vec{X}$ equal to all the possible points on the line conneting each velocity vector to the centre-of-mass motion of the cluster. The factor λ determines the cross-point. The unit vector $\hat{n}$ that we adopt satisfies $\vec{n} = \frac{\vec{v}}{|\vec{v}|}$. The vector equations of the line for sources a and b are:

$$\vec{X}_{\mathrm{a}} = \lambda_{\mathrm{a}}\hat{n}_{\mathrm{a}} + \vec{r}_{\mathrm{a}} = \lambda_{\mathrm{a}}\frac{\vec{v}_{\mathrm{a}}}{|\vec{v}_{\mathrm{a}}|} + \vec{r}_{\mathrm{a}} \tag{A1.6}$$

$$\vec{X}_{\mathrm{b}} = \lambda_{\mathrm{b}}\hat{n}_{\mathrm{b}} + \vec{r}_{\mathrm{b}} = \lambda_{\mathrm{b}}\frac{\vec{v}_{\mathrm{b}}}{|\vec{v}_{\mathrm{b}}|} + \vec{r}_{\mathrm{b}}, \tag{A1.7}$$

where $\vec{X}_{\mathrm{a}}$ need to be equal to $\vec{X}_{\mathrm{b}}$. We need to find the λ_{a} and λ_{b} values that satisfy the following condition:

$$\lambda_{\mathrm{a}} = \frac{n_{\mathrm{a}}^{\mathrm{y}}\left(r_{\mathrm{a}}^{\mathrm{x}} - r_{\mathrm{b}}^{\mathrm{x}}\right) - n_{\mathrm{b}}^{\mathrm{x}}\left(r_{\mathrm{s}}^{\mathrm{y}} - r_{\mathrm{b}}^{\mathrm{y}}\right)}{n_{\mathrm{a}}^{\mathrm{y}} n_{\mathrm{b}}^{\mathrm{x}} - n_{\mathrm{a}}^{\mathrm{x}} n_{\mathrm{b}}^{\mathrm{y}}} \tag{A1.8}$$

$$\lambda_{\mathrm{b}} = \frac{n_{\mathrm{b}}^{\mathrm{y}}\left(r_{\mathrm{a}}^{\mathrm{x}} - r_{\mathrm{b}}^{\mathrm{x}}\right) - n_{\mathrm{a}}^{\mathrm{x}}\left(r_{\mathrm{a}}^{\mathrm{y}} - r_{\mathrm{b}}^{\mathrm{y}}\right)}{n_{\mathrm{a}}^{\mathrm{y}} n_{\mathrm{b}}^{\mathrm{x}} - n_{\mathrm{a}}^{\mathrm{x}} n_{\mathrm{b}}^{\mathrm{y}}} \tag{A1.9}$$

It is important to note that these values must be negative since the normal vectors go in the direction of the velocity.

A1.4 Angle between the velocity vectors

Another fundamental parameter required for our method is the angle between each candidate pair's velocity vectors at teh cross-point. To calculate the angle between the RSs/RBs we use the following equation:

$$\theta_{\mathrm{a,b}} = \arccos \frac{\left(v_{\mathrm{x}}^{\mathrm{a}} v_{\mathrm{x}}^{\mathrm{b}} + v_{\mathrm{y}}^{\mathrm{a}} v_{\mathrm{y}}^{\mathrm{b}}\right)}{v^{\mathrm{a}} v^{\mathrm{b}}} \tag{A1.10}$$

By propagating the errors, we obtain a value corresponding to 1σ of $\theta_{1\sigma}$. Then the upper angle is obtained using:

$$\theta_{\mathrm{a,b}}^{+} = \arccos \frac{\left(v_{\mathrm{x}}^{\mathrm{a}} v_{\mathrm{x}}^{\mathrm{b}} + v_{\mathrm{y}}^{\mathrm{a}} v_{\mathrm{y}}^{\mathrm{b}}\right)}{v^{\mathrm{a}} v^{\mathrm{b}}} + \theta_{1\sigma} \tag{A1.11}$$

and the lower angle using:

$$\theta_{\mathrm{a,b}}^{-} = \arccos \frac{\left(v_{\mathrm{x}}^{\mathrm{a}} v_{\mathrm{x}}^{\mathrm{b}} + v_{\mathrm{y}}^{\mathrm{a}} v_{\mathrm{y}}^{\mathrm{b}}\right)}{v^{\mathrm{a}} v^{\mathrm{b}}} - \theta_{1\sigma} \tag{A1.12}$$

The numerator of the fraction in the above equations, $(v_{\mathrm{x}}^{\mathrm{a}} v_{\mathrm{x}}^{\mathrm{b}} + v_{\mathrm{y}}^{\mathrm{a}} v_{\mathrm{y}}^{\mathrm{b}})$, represents the dot product of the velocity vectors of objects a and b. The denominator, $v^{\mathrm{a}} v^{\mathrm{b}}$, represents the product of the magnitudes of the velocity vectors of objects a and b. Taking the fraction $\frac{v_{\mathrm{x}}^{\mathrm{a}} v_{\mathrm{x}}^{\mathrm{b}} + v_{\mathrm{y}}^{\mathrm{a}} v_{\mathrm{y}}^{\mathrm{b}}}{v^{\mathrm{a}} v^{\mathrm{b}}}$, we obtain the cosine of the angle between the two velocity vectors.

A2 Supernovae in binaries

In an star cluster, the binary SN mechanism is mainly possible via the accretion-induced collapse or implosion of a WD. In order for this to happen, it must be in a relatively compact binary such that its companion is able to overfill its Roche lobe and transfer mass to the WD. Hence, if a cluster is older than $\sim$ 100 Myr (i.e., the lifetime of the most massive stars expected to end their lives as SN due to stellar evolution alone, stars at the cluster turn-off mass are too low-mass to end their lives as SN without the additional accretion of matter in a binary (or triple).

If the binary companion that implodes is assumed to be a WD, then we can compute a maximum ejection velocity for the binary SN scenario for different companion masses and at different stages of stellar evolution (i.e., at different stellar radii). To do this, we assume that the circular binary system is in a contact state at the time of explosion, and adopt the following relation to calculate the radius of the WD (Nauenberg, 1972):

$$r_{\rm WD} = \frac{0.0225}{\mu} \cdot \left(\frac{1}{m_{\rm rel}^{2/3}} - m_{\rm rel}^{2/3} \right)^{1/2} \tag{A2.1}$$

with the mean molecular mass $\mu = 2$ as a constant and $m_{\rm WD} = 1.4$ [$M_\odot$]. The relative mass $m_{\rm rel} = \frac{m_{\rm WD}}{5.816\mu^2} = 0.24\mu^2$. Then we calculate the semi-major axis,

$$a = r_{\rm WD} + r_{\rm c}, \tag{A2.2}$$

where $r_{\rm c}$ is the radius of the companion that will be ejected. Finally, we calculate the maximum ejection velocity:

$$v_s = \sqrt{\frac{G * (m_{\rm c} + m_{\rm WD})}{a}} \tag{A2.3}$$

We use `SeBa` (Portegies Zwart and Verbunt, 1996; Nelemans et al., 2001; Toonen et al., 2012, 2018) to calculate the companion radius $r_{\rm c}$ and the maximum velocity $v_{\rm s}$. It is designed to work with the `kira` N-body integrator (Portegies Zwart and Verbunt, 2012) but can also be used independently. The module computes the

evolution of stars and binaries using a block time step scheme, which combines fixed interval updates and adaptive time step size. Fixed interval updates ensure a systematic progression of the integration and consistent updates of physical properties. The adaptive time step size adjusts based on factors like binary period, perturbations, and evolutionary state, optimizing efficiency and accuracy. We study escape velocity during WD explosion assuming a contact state. We calculate r_c using a metallicity of Z = 0.02 (solar metallicity). While high-mass stars ($M > 20[M_\odot]$) are significantly affected by metallicity due to stellar winds, the explored mass range ($M < 8[M_\odot]$) is expected to be minimally affected.

The results of this exercise are shown in Figure A2.1. The maximum velocity for each stage of stellar evolution is: Main Sequence: 408.7 km s^{-1}, Hertzsprung Gap: 350.1 km s^{-1} , Red Giant Branch: 98.3 km s^{-1}, Horizontal Branch: 114.4 km s^{-1} , Asymptotic Giant Branch: 114.3 km s^{-1}. These results highlight that old star clusters having lots of low-mass stars and white dwarfs are, in principle, capable of producing higher ejection velocities than young clusters. contribute to the high-end tail of the observed Galactic RS velocity distribution. This is because they are capable of producing the highest ejection velocities given that the progenitor binaries require WD accretors and low-mass donors ($\sim$ 1 $M_\odot$), and these can be much more compact than binaries with massive companions that detonate instead by reaching the end of their lives.

In general, we expect RSs coming from old star clusters formed from the SN-induced mechanism to have low probabilities of being associated with a host cluster, due primarily to a lack of other metrics to establish them as RSs associated with a progenitor cluster (a limitation that the triple disintegration scenario does not suffer from). For the SN mechanism, the best case scenario for observationally identifying RSs coming from old clusters is when 3D velocities are available, such that the point of origin can be determined with confidence. Apart from this, the chemical composition and location of RS candidates in a colour-magnitude diagram are all that observers have to work with (assuming that no possibly associated SN remnant is identifiable in the host cluster, which is generally the case for old clusters), although several studies have had success using chemical tagging, such as Ness et al., 2018, Price-Jones et al., 2020, Grondin et al., 2022 and Casamiquela et al., 2021. Relative to the SN-based mechanism, RSs formed from the disintegration of three- and four-body systems should in principle be

detectable with much higher confidence, due to additional constraints coming from timescale as well as energy and momentum conservation-based arguments that can be folded into the analysis by searching for a counterpart recoiled RB.

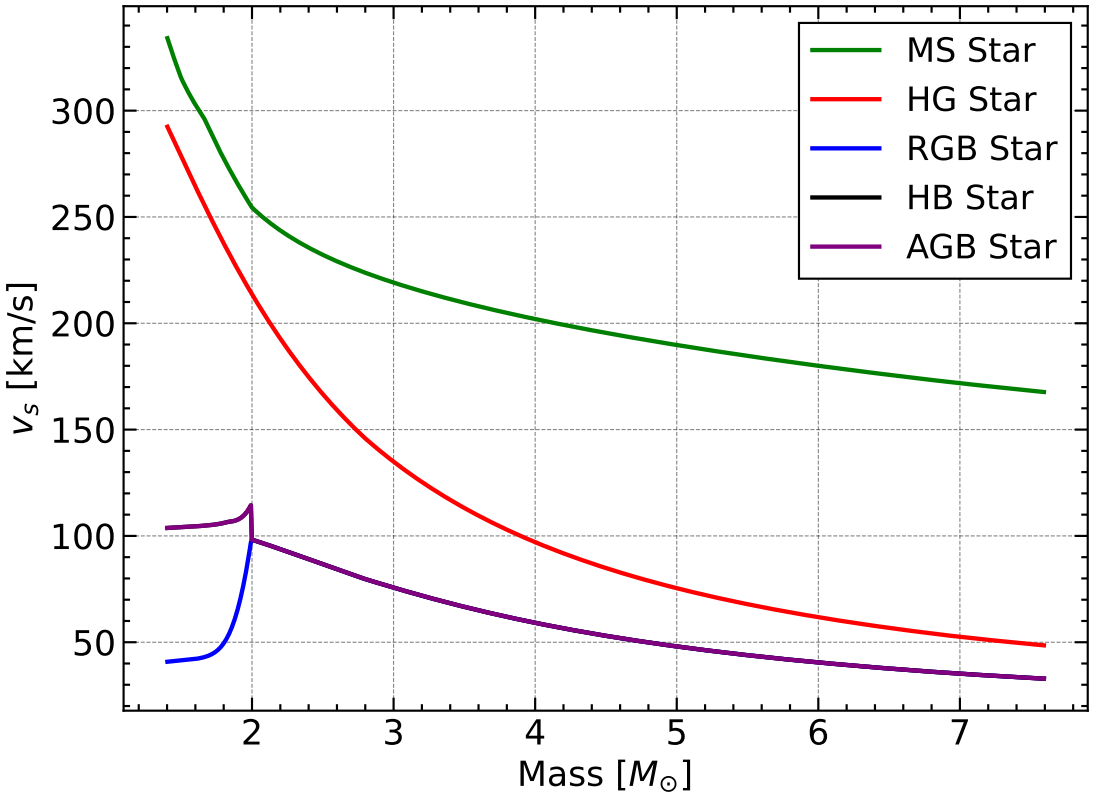

Figure A2.1: Maximum ejection velocities after a supernova explosion in a binary system. Both stars are assumed to be in a contact state at the time of explosion. One of the stars is assumed to be a white dwarf with 1.4 $M_\odot$ and the other star varies in mass (and hence radius), as shown on the x-axis. The companion radius as a function of mass is computed using the `SeBa` code, as described in the text. Note that the curve for the Horizontal Branch is plotted underneath that for the Red Giant Branch and can be difficult to discern.